RESEARCH ARTICLE SUMMARY

CANCER IMMUNOLOGY

CD5 expression by dendritic cells directs T cell immunity and sustains immunotherapy responses

Mingyu He, Kate Roussak, Feiyang Ma, Nicholas Borcherding, Vince Garin, Mike White, Charles Schutt, Trine I. Jensen, Yun Zhao, Courtney A. Iberg, Kairav Shah, Himanshi Bhatia, Daniel Korenfeld, Sabrina Dinkel, Judah Gray, Alina Ulezko Antonova, Stephen Ferris, David Donermeyer, Cecilia Lindestam Arlehamn, Matthew M. Gubin, Jingqin Luo, Laurent Gorvel, Matteo Pellegrini, Alessandro Sette, Thomas Tung, Rasmus Bak, Robert L. Modlin, Ryan C. Fields, Robert D. Schreiber, Paul M. Allen, Eynav Klechevsky*

INTRODUCTION: Immune checkpoint blockade (ICB) therapy that blocks inhibitory T cell checkpoint molecules such as programmed cell death protein 1 (PD-1) and cytotoxic T lymphocyte–associated protein 4 (CTLA-4) has revolutionized cancer treatments. Despite its efficacy, half of the treated patients respond poorly and experience disease progression after therapy. To further improve immunotherapy outcome, a better understanding of the immune landscape and the tumor microenvironment (TME) is needed. In this context, dendritic cells (DCs), a functionally diverse system of antigen-presenting cells, play an instrumental role in eliciting antitumor responses during ICB therapy by inducing de novo $CD8^+$ cytotoxic and $CD4^+$ helper T cells against cancer-specific antigens. However, the specific DC features that are critical for driving effective T cell immunity and how subset composition in the tissue affects responsiveness to therapy remain unresolved.

RATIONALE: CD5, which is a transmembrane glycoprotein expressed on the surfaces of conventional T cells and some B cells, was recently recognized as a marker of a subset of DCs in both mice and humans. CD5 plays an important role in fine-tuning T cell receptor signaling during development and in their effector function in the periphery. However, the physiological roles of CD5 on DCs and the impact of such $CD5^+$ DCs on tumor immunity remain unclear. In our previous work, we showed that migratory $CD5^+$ DCs in the human skin prime helper T cells and multifunctional cytotoxic T cells more effectively than DCs that lack CD5. We hypothesized that the increased frequency of $CD5^+$ DCs in inflammatory settings correlates with their involvement in antitumor responses and responses to ICB therapy.

RESULTS: We investigated the mechanisms that underlie DC-mediated effector T cell priming, focusing on the role of CD5 expressed by these interacting cells. We analyzed the myeloid compartment of human skin draining lymph nodes and found that the frequency of the $CD5^+$ DC population within the DC2 compartment was reduced in human melanoma-affected lymph nodes compared with the same population in unaffected tissue. Accordingly, *CD5* expression as well as a $CD5^+$ DC gene signature correlated with greater survival and relapse-free survival in patients with a variety of cancers, including melanoma. We identified a critical immunostimulatory function for CD5 on DCs that potentiates the priming of tumor-reactive T cell activation, proliferation, effector function, and response to ICB therapy. The expression of CD5 on DCs correlated directly with the extent of effector helper $CD4^+$ and cytotoxic T cell priming in humans. Selective deletion of CD5 expression in DCs prevented an efficient response to ICB therapy in tumor-bearing mice, resulting in defective immune rejection of tumors. This defect correlated with the activation of $CD5^{lo}$ T cells, including $CD5^{lo}CD4^+$ T cells and neoantigen-specific $CD5^{lo}CD8^+$ T cells with poor effector function. In parallel, we examined biopsies of patients with melanoma and found that $CD5^{hi}$ Tcell frequencies aligned with the $CD5^+$ DC density. Similarly, deletion of CD5 expression in T cells negatively affected $CD5^+$ DC-mediated T cell priming, antitumor immunity, and the response to ICB. Moreover, we found increased numbers of $CD5^+$ DCs after ICB in vivo, which corresponded to increased numbers of these cells in a patient with *PD-1* deficiency. Furthermore, interleukin-6 (IL-6), which was abundant in the cells of this patient, was also detected at higher levels within tumors after ICB therapy compared with baseline measurements. Correspondingly, we identified IL-6 as an important factor in $CD5^+$ DC differentiation and survival.

CONCLUSION: Our data provide insight into how immunotherapies like ICB work and identify CD5 on DCs as a new potential target for enhancing response rates among patients undergoing treatments. The role of DC CD5 in engaging effective antitumor immunity provides one explanation for the correlation of human DC2s, the only conventional DC subpopulation in humans that expresses CD5, with effector helper T cell density in tumors and with the patient responsiveness to ICB therapy. Overall, increased $CD5^+$ DCs in human lymphoid tissue aligns with markers of effector T cell quality, as well as with patient overall survival. Thus, harnessing CD5 on DCs may be a promising avenue for enhancing the efficacy of immunotherapy against multiple tumors. ■

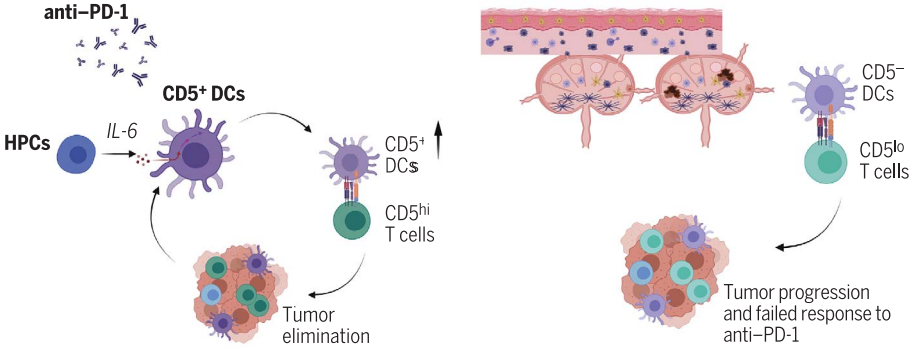

DC CD5 directs the response to immunotherapy. $CD5^+$ DC frequency was reduced in tumor-affected lymph nodes, and their presence correlated with greater patient survival in multiple tumors. $CD5^+$ DC numbers increased during ICB therapy, and low IL-6 concentrations promoted their de novo differentiation. The requirement for CD5 on DCs was linked to the priming of effector $CD5^{hi}$T cells and optimal ICB therapy. [Figure created with Biorender.com]

The list of author affiliations is available in the full article online.
*Corresponding author. Email: eklechevsky@wustl.edu
Cite this article as M. He *et al.*, *Science* **379**, eabg2752 (2023). DOI: 10.1126/science.abg2752

RESEARCH ARTICLE

CANCER IMMUNOLOGY

CD5 expression by dendritic cells directs T cell immunity and sustains immunotherapy responses

Mingyu He[1], Kate Roussak[1], Feiyang Ma[2], Nicholas Borcherding[1], Vince Garin[1], Mike White[1], Charles Schutt[1], Trine I. Jensen[3], Yun Zhao[1], Courtney A. Iberg[1], Kairav Shah[1], Himanshi Bhatia[1], Daniel Korenfeld[1], Sabrina Dinkel[1], Judah Gray[1], Alina Ulezko Antonova[1], Stephen Ferris[1], David Donermeyer[1], Cecilia Lindestam Arlehamn[4], Matthew M. Gubin[1], Jingqin Luo[5], Laurent Gorvel[1], Matteo Pellegrini[2], Alessandro Sette[4,6], Thomas Tung[7], Rasmus Bak[3,8], Robert L. Modlin[9,10], Ryan C. Fields[4], Robert D. Schreiber[1], Paul M. Allen[1], Eynav Klechevsky[1]*

The induction of proinflammatory T cells by dendritic cell (DC) subtypes is critical for antitumor responses and effective immune checkpoint blockade (ICB) therapy. Here, we show that human CD1c$^+$CD5$^+$ DCs are reduced in melanoma-affected lymph nodes, with CD5 expression on DCs correlating with patient survival. Activating CD5 on DCs enhanced T cell priming and improved survival after ICB therapy. CD5$^+$ DC numbers increased during ICB therapy, and low interleukin-6 (IL-6) concentrations promoted their de novo differentiation. Mechanistically, CD5 expression by DCs was required to generate optimally protective CD5^{hi} T helper and CD8$^+$ T cells; further, deletion of CD5 from T cells dampened tumor elimination in response to ICB therapy in vivo. Thus, CD5$^+$ DCs are an essential component of optimal ICB therapy.

Immunotherapy has revolutionized cancer treatment. Melanoma is a prominent example of immune checkpoint blockade (ICB) success, with more than 50% of patients responding to dual anti–programmed cell death protein 1 (PD-1) and anti–cytotoxic T lymphocyte–associated protein 4 (CTLA-4) regimens (*1*, *2*). However, this leaves nearly 50% of patients as primary nonresponders, and most of these patients will experience disease progression after therapy. To improve the benefit of immunotherapy in patients with melanoma and to extend the success to other more immunotherapy-refractory cancers (for example, immunologically "cold" tumors such as pancreatic cancer), a better understanding of the immune landscape and tumor microenvironment (TME) is needed.

[1]Department of Pathology and Immunology, Washington University School of Medicine, St. Louis, MO 63110, USA. [2]Molecular Cell and Developmental Biology at University of California, Los Angeles (UCLA), Los Angeles, CA 90095, USA. [3]Department of Biomedicine, Aarhus University, 8000 Aarhus C, Denmark. [4]Center for Infectious Disease and Vaccine Research, La Jolla Institute for Immunology, La Jolla, CA 92037, USA. [5]Department of Surgery, Washington University School of Medicine, St. Louis, MO 63110, USA. [6]Department of Medicine, Division of Infectious Diseases and Global Public Health, University of California San Diego (UCSD), La Jolla, CA 92037, USA. [7]Department of Surgery, Division of Plastic and Reconstructive Surgery, Washington University School of Medicine, St. Louis, MO 63110, USA. [8]Aarhus Institute of Advanced Studies (AIAS), Aarhus University, 8000 Aarhus C, Denmark. [9]Division of Dermatology, Department of Medicine, David Geffen School of Medicine at UCLA, Los Angeles, CA 90095, USA. [10]Department of Microbiology, Immunology and Molecular Genetics, David Geffen School of Medicine at UCLA, Los Angeles, CA 90095, USA.
*Corresponding author. Email: eklechevsky@wustl.edu

Dendritic cells (DCs) play critical roles in antitumor immunity by inducing effector T cell responses against cancer-specific and cancer-associated antigens, many of which are relatively poorly immunogenic (*3*). Tumor cells, however, hijack the immune system, causing T cell exhaustion and DC dysfunction. Cancer-induced T cell exhaustion may be reversed through checkpoint blockade; however, this treatment fails to show clinical benefit in many patients, is unsuccessful for some cancer types, and can have severe side effects that limit its use.

Conventional DCs (cDCs) are broadly divided into cDC1 and cDC2 populations that arise through distinct pre-DC lineages (*4*). cDCs either reside in the lymph node (LN) or migrate in from peripheral tissues, such as the skin (*5*). Through their specific surface receptors and cytokines and through their differential use of antigen processing and presentation pathways, distinct DC subsets take specialized roles for activating different modes of immunity (*6*–*8*). For example, human skin harbors Langerhans cells in the epidermis and CD1a$^+$CD1c$^+$ or CD14-expressing DCs in the dermis. Whereas migratory Langerhans cells and dermal CD1a$^+$CD1c$^+$ DCs prime helper T cells (*6*, *9*) and cross-prime cytotoxic T lymphocytes (CTLs) (*6*, *7*, *10*), the dermal CD14$^+$ DCs promote humoral immunity (*6*, *11*) but inhibit CTLs (*6*, *7*) and prime regulatory T cells (*12*).

Both human and murine cDC1s comprise a relatively homogeneous population (*13*), whereas cDC2s are more heterogeneous. cDC2s are defined by the cell surface expression of CD11b, DCIR-2, and CD172a [signal regulatory protein alpha (SIRP-α)] (*14*, *15*) in mice and CD1c and Clec10A in humans (*13*), with differential surface expression of Esam, Mgl2 (CD301b, the mouse homolog to Clec10A) (*16*), or CLEC12A (*17*) in mice and CD5 in humans (*18*, *19*). Both cDC1s and cDC2s contribute to antitumor immunity by priming CTL responses and CD4$^+$ helper T (T_H) cells, respectively. Yet despite such understanding of the functions elicited by distinct DC subsets (*5*), our knowledge of the DC subset or subsets that promote the most potent antitumor responses in humans is less clear. We previously reported that migratory skin CD5$^+$ DCs, which we found on a subset of DC2s, prime inflammatory T_H cells and multifunctional CTLs more effectively than their CD5$^-$ DC2 counterparts (*18*, *20*). Their increased frequency in inflammatory settings led us to hypothesize that these cells are predominantly involved in the antitumor response.

CD5 is a type I transmembrane glycoprotein that is expressed on the surface of T cells and a subset of B cells. Additionally, it is now accepted as a marker of a subset of DC2s (CD1c$^+$ DCs) in humans (*18*, *19*, *21*). Although CD5 was initially detected on murine DCs in the early 1990s (*15*, *22*–*24*), its physiological role is not fully understood. Whereas some studies of murine cells indicated that CD5 functions as an inhibitory molecule (*25*–*29*), others suggested that when expressed on mature T cells, CD5 can promote T cell activation, interleukin-2 (IL-2) production (*30*–*33*), and pathogenic T_H17 cell differentiation (*25*, *34*, *35*) and can also confer a nuclear factor κB (NF-κB)–dependent survival advantage (*36*). Thus, the functional relevance of CD5 remains unresolved and may vary with cell type or microenvironment to promote a specific functional outcome (*37*).

Here, we identified a critical immunostimulatory function for CD5 on DCs that potentiates the priming of effector T cells. CD5 expression on DCs correlated with greater overall survival and relapse-free survival in patients with melanoma, lung squamous cell carcinoma, sarcoma, breast cancer, cervical squamous cell carcinoma, and endocervical adenocarcinoma, and the frequency of CD5$^+$ DCs was reduced 20-fold in human melanoma-affected LNs compared with unaffected tissue. Further, using conditional deletion of CD5 on DCs in mice, we found resistance to ICB therapy in sarcoma and colorectal cancer tumor models. The requirement for CD5 on DCs was linked to the activation of CD5^{hi}CD4$^+$ T cells and neoantigen-specific CD5^{hi}CD8$^+$ T cells. These data suggest that CD5 expression on cells of the myeloid compartment plays a key role in determining the outcomes of naturally occurring immune responses to cancer and that harnessing CD5 on DCs may be a promising avenue for enhancing the efficacy of ICB therapy against multiple tumors.

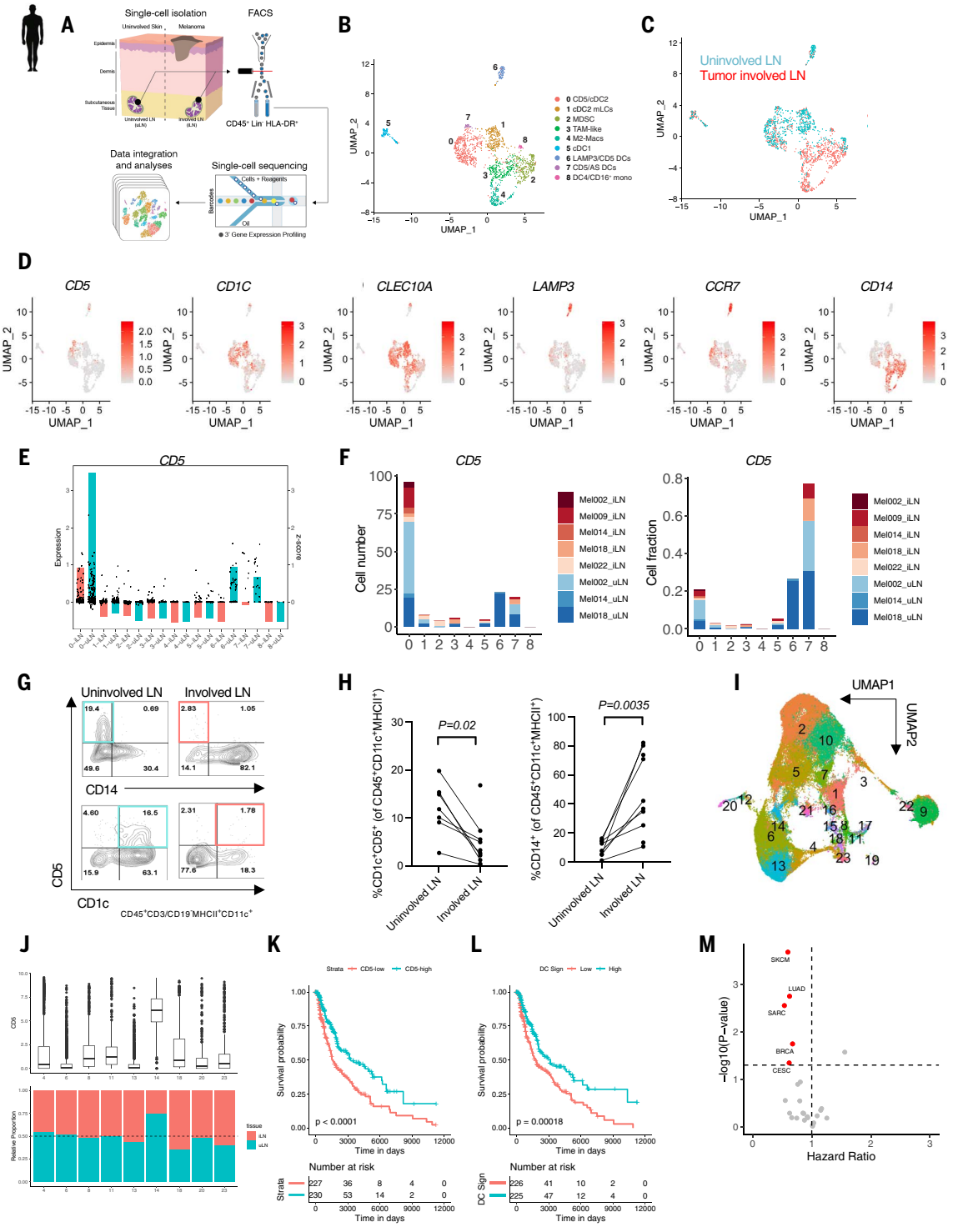

Fig. 1. Altered distribution of CD1c$^+$CD5$^+$ DCs in melanoma-affected human LNs and correlation with patient survival. (**A**) Workflow for single-cell analysis of myeloid cells from human melanoma that were isolated from five iLNs and three matched uLNs from patients with melanoma. (**B**) UMAP displaying nine clusters of myeloid CD45$^+$lineage$^-$HLA-DR$^+$ cells sorted from five iLNs and three matched uLNs from patients with melanoma and processed for scRNA-seq using 10× Genomics technology (see also fig. S1, A and B). MDSC, myeloid-derived suppressor cell; TAM, tumor-associated macrophage. (**C**) UMAP displaying CD45$^+$lineage$^-$ HLA-DR$^+$ cell distribution based on tissue type. (**D**) UMAP plots of six marker genes associated with various myeloid cell types in human tumor iLNs and uLNs as defined in Fig. 1, B and C. The color scale represents the normalized expression of the gene. (**E**) Scatter plot showing the *z*-score based on the total expression of CD5 for each cluster separated by iLN (red) and uLN (blue). The left *y* axis corresponds to the dots on the plot, which represent the expression of CD5 in individual cells. The right *y* axis corresponds to the bars. The height of each bar represents the *z*-score of the gene in the group of cells of each cluster. (**F**) Bar plots showing the number of cells expressing CD5 in each cluster (left) and the fraction of cells in each cluster and sample that expresses CD5 (right). Colors represent the samples from which the cells were derived. Shades of blue or red indicate uLNs or iLNs from different donors, respectively. (**G**) Expression of CD1c$^+$CD5$^+$ (bottom) and CD14$^-$CD5$^+$ (top) in iLNs and uLNs of representative patient Mel002. Cells were

gated on CD45$^+$CD3$^-$CD19$^-$MHCII$^+$CD11c$^+$. One representative plot of eight patients is shown. (**H**) CD1c$^+$CD5$^+$ (left) and CD14$^+$CD5$^-$ (right) in eight iLNs and matched uLNs, plus an additional two iLNs from patients with melanoma. Symbols indicate values from individual patients. (**I**) UMAP displaying CyTOF analysis of CD45$^+$ cells from four iLNs and matched uLNs of patients with melanoma. (**J**) Relative expression of CD5 in each myeloid cell–specific cluster (top) and distribution among the iLN and uLN cells (bottom). For the box-and-whisker plots, the bars are the default setting using interquartile ranges (IQR), where the lower whisker is quartile 1 minus 1.5 × IQR and the upper whisker is quartile 3 plus 1.5 × IQR. (**K**) Kaplan-Meier curve (top) showing the proportion of overall survival across the TCGA melanoma cohort by median *CD5* mRNA level, as generated by RNA-seq, comparing *CD5*-high (blue) versus *CD5*-low (red). Strata (bottom) refers to grouping, high versus low. (**L**) Kaplan-Meier curve (top) showing the proportion of overall survival across the TCGA melanoma cohort by median CD5$^+$ DC signature mRNA level comparing CD5$^+$DC-high (blue) versus CD5$^+$DC-low (red). DC signature (DC Sign) (bottom) was developed using the product of *CD5*, *CD1C*, *LAMP3*, and *CLEC10A* divided by the mRNA level of *CD3G*. (**M**) Volcano plot of the hazard ratios versus −log10(*P* value) across TCGA cohorts for the CD5$^+$ DC signature. Points highlighted in red are significantly ($P < 0.05$) associated with worse overall survival. SKCM, skin cutaneous melanoma; LUAD, lung adenocarcinoma; SARC, sarcoma; BRCA, breast invasive carcinoma; CESC, cervical squamous cell carcinoma and endocervical adenocarcinoma.

Results

CD5 expression correlates with improved disease prognosis in patients with melanoma

After identifying CD5$^+$ DCs in migratory skin DCs (*18*), we queried myeloid heterogeneity in the skin tumor-draining lymph nodes (TDLNs) of patients with metastatic melanoma. We sorted CD45$^+$lineage (CD3/CD56/CD19)$^-$major histocompatibility complex (MHC) II$^+$ antigen-presenting cells from five tumor-affected and three unaffected LNs that drain the skin of a melanoma patient (table S1) and performed single-cell RNA sequencing (scRNA-seq) using the 10× Genomics Chromium platform paired with deep sequencing. Uniform manifold approximation and projection (UMAP) analysis of 1596 TDLN myeloid cells from all the integrated samples (Fig. 1A and fig. S1A) yielded nine high-quality and distinct population clusters (designated clusters 0 to 8; Fig. 1B). Clusters 0, 1, 6, and 7 were expressed mainly in tumor-free tissue (Fig. 1, B and C, and fig. S1, A and B), whereas clusters 2, 3, 4, and 8 were principally present in tumor-affected tissue (Fig. 1, B and C, and fig. S1, A and B). We used gene overlays of individual canonical myeloid markers to further identify the cell clusters (Fig. 1D). Clusters 0, 1, and 6 contained CD1c- and CLEC10A-expressing DC populations, representing the cDC2 subset (*13*). Cluster 6 shared genes with lysosome-associated membrane glycoprotein 3 (LAMP3) DCs (*38*) as well as the recently described mature DCs enriched in immunoregulatory molecules (mreg) DCs, with the exception of *IL4R*, *STAT6*, and *AXL*, which were absent in LN cluster 6 DCs but present in mregDCs and which were required for their suppressive activity (*39*) (fig. S1, C and D). Cluster 7 contained progenitor pre-DC/AXL$^+$SIGLEC6$^+$ DCs, which express *AXL*, *SIGLEC6*, and *IL3RA*. We found that *CD5* transcript expression corresponded with cells in the tumor-uninvolved tissue (Fig. 1, E and F)—mainly the CD1c$^+$CLEC10A$^+$ cDC2s in clusters 0, 6, and 7—and was concordant with the expression of *LAMP3* and *CCR7* (Fig. 1D); these findings were in accordance with the known biology of migratory skin DCs (*40*). A subset of migratory Langerhans cells, identified by the expression of CD1a (*CD1A*), *CD1C*, and *CD207*, was present in cluster 1 (fig. S1E) and was also identified using cytometry by time of flight (CyTOF) (in myeloid cluster 16; fig. S1, F and G). XCR1$^+$CLEC9A$^+$ cells (cDC1s) occupied cluster 5 and were present in both tumor-involved and uninvolved tissues (Fig. 1, B and C, and fig. S1, E and H). Macrophages and monocyte-derived cells occupied clusters 2, 3, 4, and 8 and were enriched in melanoma-involved tissue, with cluster 2 cells expressing *THBS1* and the *S100A* family members *VCAN* and *FCN1*, which are characteristic of myeloid-derived suppressor cell–like cells. Clusters 3 and 4 contained triggering receptor expressed on myeloid cells 2 (*TREM2*)–expressing macrophages, tumor-associated macrophage–like and M2 macrophages (Fig. 1B and fig. S1, E and H), which also expressed *CD206/MRC1* (higher on cluster 3) and *C1QA*, *C1QB*, and *APOE* (higher on cluster 4) (fig. S1, E and H). Cluster 8 corresponded to nonclassical CD16$^+$ monocytes (DC4) that expressed CD16 (*FCGR3A*), *C5AR1*, *S100A4*, and *LILRB2* (fig. S1H).

We next assessed the presence of CD1c$^+$CD5$^+$ DCs in eight tumor-involved LNs (iLNs) and patient-matched uninvolved LNs (uLNs) by flow cytometry and CyTOF. We observed that these cells were restricted to a uLN and reduced in a metastatic tumor LN (mean percentage ± SEM; 13.5 ± 2.5% versus 4.0 ± 1.0%) [Fig. 1, G (bottom) and H (left)]. This contrasted with the CD14$^+$ cells, which preferentially occupied tumor-affected tissue and had no CD5 expression (9.2 ± 3.6% versus 55.2 ± 13.8%) [Fig. 1, G (top) and H (right)]. UMAP analysis showed that CD5-expressing DCs occupied a distinct myeloid cluster 14, which was enriched in uLNs (Fig. 1, I and J, and table S2).

We then examined the association of CD5 with disease prognosis based on The Cancer Genome Atlas (TCGA) melanoma cohort that is composed of 469 patients. *CD5* expression (Fig. 1K) and the CD5$^+$ DC signature (Fig. 1L) were associated with favorable prognosis for melanoma. There was no correlation between CD5 expression and patient age or disease staging, as measured by Clark level (fig. S2, A and B). Furthermore, the CD5$^+$ DC signature in tumors correlated with survival in an independent melanoma cohort (*41*) (fig. S2C). In addition to cutaneous melanoma, the CD5$^+$ DC signature was associated with favorable prognosis of lung squamous cell carcinoma, sarcoma, breast cancer, cervical squamous cell carcinoma, and endocervical adenocarcinoma (Fig. 1M). As expected, *CD5* correated with the expression of *CD1c* [coefficient of determination (R^2) = 0.53], *LAMP3* (R^2 = 0.51), *CLEC10A* (R^2 = 0.65), *CD40* (R^2 = 0.48), and *CLEC9A* (R^2 = 0.6) but was poorly correlated with *TREM2*, *THBD*, and *AXL* expression in the tumor (fig. S2D). Overall, CD5$^+$ DCs were enriched in the tumor-free LNs, and their presence was associated with better prognosis for patients with melanoma, lung squamous cell carcinoma, sarcoma, breast cancer, cervical squamous cell carcinoma, and endocervical adenocarcinoma.

CD5$^+$ DCs isolated from LNs and skin efficiently prime allogeneic naïve T cell responses

DCs are distinctive in their capacity to induce proliferation of allogeneic naïve CD4$^+$ T cells and CD8$^+$ T cells in a mixed lymphocyte reaction (*42*). Within this diverse cell system, we previously identified a subset of cells that express CD5 within the migratory dermal CD14$^-$CD141$^-$CD1c$^+$ DCs and epidermal Langerhans cells (*18*). The dermal CD5$^+$ DCs (fig. S3A) were powerful stimulators of naïve CD4$^+$ T and CD8$^+$ T cell proliferation (Fig. 2A). As few as 1000 of these cells were sufficient to induce nine and seven cell divisions within the CD4$^+$ T cell (Fig. 2B, left) and CD8$^+$ T cell (Fig. 2B, right) populations, respectively, whereas the CD5$^-$ dermal DCs induced only four and two divisions, respectively (Fig. 2B). Similarly, CD1c$^+$CD5$^+$ LN DCs (fig. S3B) were stronger stimulators of naïve CD4$^+$ and CD8$^+$ T cell proliferation than their CD1c$^+$CD5$^-$ counterparts (Fig. 2, A and B). The enhanced capacity of LN CD5$^+$ DCs to activate T cells was reflected in the amounts of cytokines that were produced in the primed T cell cultures (Fig. 2, C and D). Compared with LN CD5$^-$ DCs, CD5$^+$ DCs isolated from LNs induced more interferon-γ (IFN-γ) and tumor necrosis factor–α (TNF-α) production by naïve CD4$^+$ T cells (Fig. 2C, left) and CD8$^+$ T cells (Fig. 2C, right). Moreover, higher amounts of TNF-α were detected in cocultures of T cells activated by LN CD5$^+$ DCs (Fig. 2D, left) or dermal CD5$^+$ DCs (Fig. 2D, right) compared with those detected in cocultures of T cells and CD5$^-$ DCs or CD14$^+$ cells (Fig. 2D). CD5$^+$ DC–primed T cells also yielded higher amounts of IFN-γ than those primed by the other LN-specific

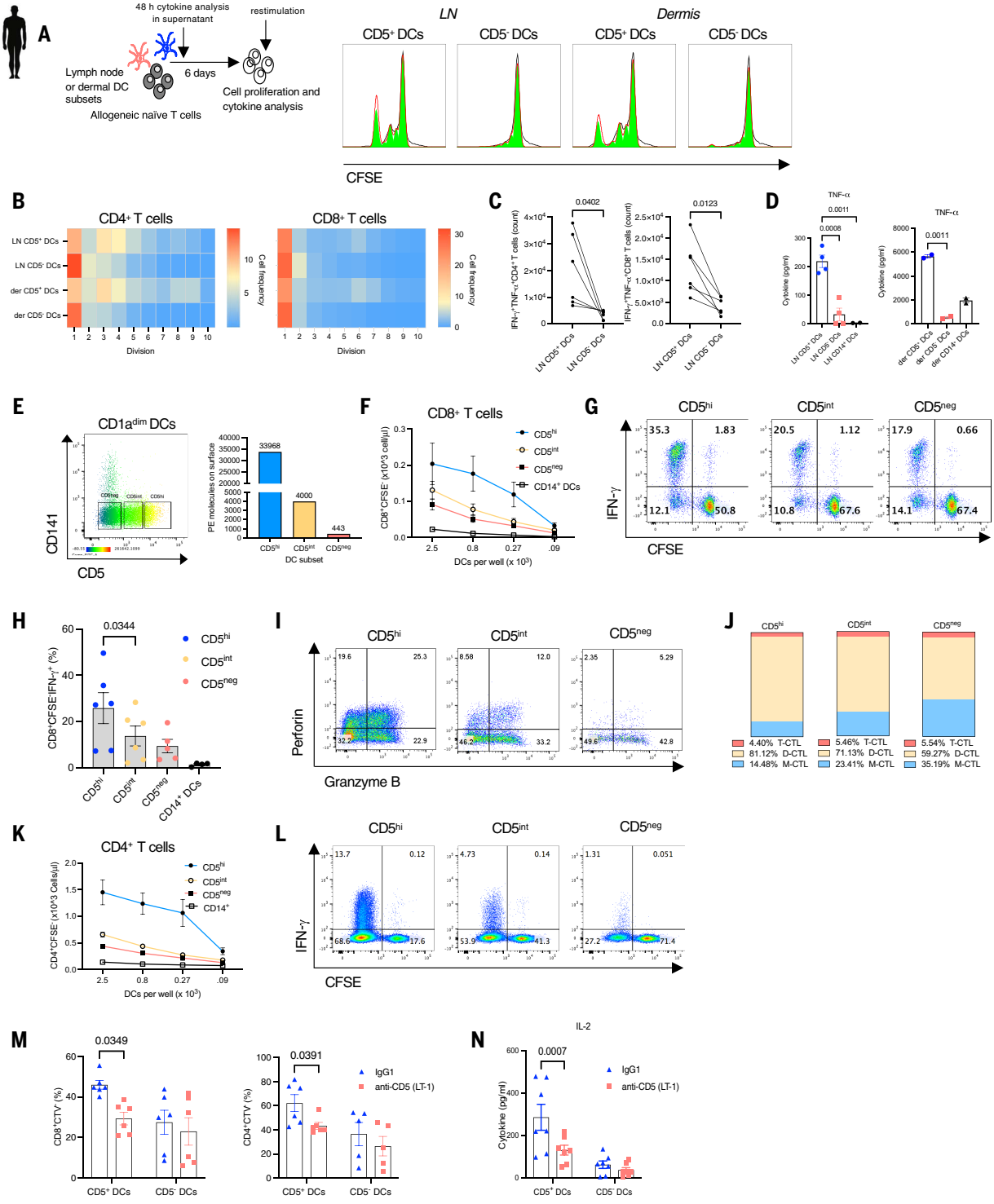

Fig. 2. CD5 expression on DCs correlates with CD4$^+$ and CD8$^+$ T cell activation. (**A**) CFSE dilution of allogeneic naïve T cells primed by either CD5$^+$ or CD5$^-$ DCs isolated from an uLN from a patient with melanoma or from healthy human dermis. Representative results of three melanoma LN donors and at least 10 dermal DC donors are shown. (**B**) Proliferation index of allogeneic naïve CD4$^+$ T cells (left) and CD8$^+$ T cells (right) primed by CD5$^+$ or CD5$^-$ LN DCs or CD5$^+$ and CD5$^-$ dermal (der) DCs. Representative results of three melanoma LN donors and at least 10 dermal DC donors are shown. The color scale represents the fraction of cells that have diluted CFSE in each of the indicated cell divisions. (**C**) Number of IFN-γ$^+$TNF-α$^+$ CD4$^+$ T cells (left) and CD8$^+$ T cells (right) primed by CD5$^+$ or CD5$^-$ LN DCs. Composite data of three experiments with three LN donors are shown. (**D**) TNF-α production measured in the cultures of T cells stimulated by CD5$^+$ or CD5$^-$ LN DCs (left) or CD5$^+$ or CD5$^-$ dermal DCs (right) or by control CD14$^+$ DCs for 48 hours. Composite data of two experiments with two LN donors and two different dermal donors are shown. Data represent the means ± SEM. (**E**) Flow cytometric gating scheme showing CD5^{hi}, CD5^{int}, and CD5^{neg} DCs (live, lineage$^-$HLA-DR$^+$CD11c$^+$CD14$^-$CD1a^{dim}) (left). See also fig. S3A. Quantification of surface CD5 expression (right) on CD5^{hi}, CD5^{int}, and CD5^{neg} dermal DCs using BD QuantiBrite beads. One representative quantification of three performed with DCs from three different donors is shown. PE, phycoerythrin. (**F**) Sorted

dermal CD5^{hi} (blue), CD5^{int} (yellow), and CD5^{neg} (red) DCs or control CD14$^+$ DCs (black) were cocultured with naïve CD8$^+$ T cells at different DC:T cell ratios for 6 days before CD8$^+$ T cell numbers were determined using BD TruCOUNT beads. Composite data of three experiments performed with three different donors are shown; data represent means ± SEM. (**G**) IFN-γ expression by the proliferating CD8$^+$ T cells primed by dermal CD1a$^{(dim)}$ CD5^{hi}, CD5^{int}, or CD5^{neg} DCs. One experiment of six performed with six different donors is shown. (**H**) Composite data of six experiments performed with six different donors are shown; data represent means ± SEM. (**I**) Granzyme B and perforin expression by proliferating (CFSE^{lo}) CD8$^+$ T cells primed by CD5^{hi}, CD5^{int}, or CD5^{neg} DCs. One experiment of three performed with three different donors is shown. (**J**) Proportions of T-CTLs, D-CTLs, and M-CTLs induced by dermal CD1a$^{(dim)}$ CD5^{hi}, CD5^{int}, or CD5^{neg} DCs. Composite data of three experiments with three different donors are shown. (**K**) Activated CD4$^+$ T cell proliferation in response to different numbers of dermal CD1a$^{(dim)}$ CD5^{hi} (blue), CD5^{int} (yellow), and CD5^{neg} (red) DCs and CD14$^+$ (black) DCs. CD4$^+$ T cells were determined on day 6 using BD Trucount beads. Composite data of four experiments with four different donors are shown; data represent means ± SEM. (**L**) Expression of IFN-γ by proliferating CD4$^+$ T cells primed by dermal CD1a$^{(dim)}$ CD5^{hi}, CD5^{int}, or CD5^{neg} DCs. One experiment of three performed with three different donors is shown. (**M**) Proliferation of CD8$^+$ (left) and CD4$^+$ T cells (right) after stimulation with CD5$^+$ and CD5$^-$ DCs and anti-CD5 blocking mAb. Composite data of two experiments performed with two different donors in triplicates are shown. CTV, CellTrace Violet proliferation dye. (**N**) IL-2 production measured in the culture supernatant of T cells after stimulation with CD5$^+$ or CD5$^-$ DCs in the presence or absence of anti-CD5 blocking mAb (LT-1). Composite data of three experiments performed with three different donors in duplicates or triplicates is shown; data represent means ± SEM. In (C), (D), (H), (M), and (N), the numbers over the brackets are *P* values.

DC subsets [CD5$^-$CD206$^-$, CD206$^+$CD5$^-$ DCs, or XCR1$^+$ DCs] (fig. S3, C and D). Other lymphoid organs tested, including spleen and tonsils, showed only scarce numbers of CD5$^+$ DCs compared with LNs (fig. S3, E and F). Thus, LN CD1c$^+$CD5$^+$ DCs may populate migrating skin DCs and share a functional similarity with the dermal CD1c$^+$CD5$^+$ DCs in potentiating CD4$^+$ and CD8$^+$ T cell priming.

CD5$^+$ DCs efficiently reactivate immunity

We next assessed the role of CD1c$^+$CD5$^+$ DCs in reactivating influenza matrix protein M1 (Flu-M1)–specific CD8$^+$ T cells. CD1c$^+$CD5$^+$ DCs or CD1c$^+$CD5$^-$ DCs, as well as CD14$^+$ DCs, were isolated from the dermis of human leukocyte antigen (HLA)–A2$^+$ donors and loaded with an 18–amino acid peptide that contains an HLA-A2–restricted epitope (amino acids 58 to 66) derived from Flu-M1. The DCs were cultured with autologous CD8$^+$ T cells isolated from blood, and the expansion of Flu-M1–specific CD8$^+$ T cells was analyzed after 8 days by using a specific MHC tetramer (fig. S4A). CD5$^+$ DCs were notably more efficient at inducing greater numbers of antigen-specific CD8$^+$ T cells than CD5$^-$ DCs or CD14$^+$ DCs (12.6 ± 6.57% versus 2.85 ± 1.45% versus 0.65 ± 0.3%) (fig. S4B). The enhanced capacity to reactivate CD8$^+$ T cells was not restricted to HLA-A2. CD5$^+$ DCs purified from the dermis and cultured with autologous CD8$^+$ T cells in the presence of MHC I–restricted peptides from Epstein-Barr irus and cytomegalovirus induced more effector (granzyme B–producing) CD8$^+$ T cells than did CD5$^-$ and CD14$^+$ DCs (fig. S4C, left). Measurement of IFN-γ production showed that dermal CD1a$^{(dim)}$ CD5$^+$ DCs activated twofold-stronger antigen-specific responses than their dermal CD1a$^{(dim)}$ CD5$^-$ counterparts (fig. S4C, right). Similar results were obtained upon measurement of IFN-γ release by CD8$^+$ T cells in response to an MHC I–restricted peptide pool [fig. S4, D (left) and E]. A related approach revealed the greater efficiency of CD5$^+$ DCs in activating MHC II–restricted viral-specific CD4$^+$ T cell responses [fig. S4, D (right) and E]. Collectively, CD5$^+$ DCs were potent inducers of antigen-specific memory CD8$^+$ and CD4$^+$ T cells against tumor-associated viral antigens.

CD5 expression on DCs correlates with T cell priming

To determine the impact of CD5 expression by DCs on the priming of effector T cells, we sorted the dermal CD1c$^+$ DCs based on CD5 expression (CD5^{hi}, CD5^{int}, and CD5^{neg} DCs) (Fig. 2E, left). Using a directly conjugated primary monoclonal antibody (mAb) and Quantibrite quantification beads, we estimated that CD5^{hi} DCs (blue) expressed ~10 times more CD5 molecules than the CD5^{int} DCs and ~100 times more than the CD5^{neg} DCs (Fig. 2E, right). After a 6-day coculture, we found that allogeneic naïve CD8$^+$ T cell expansion (percentages and numbers) was more effectively primed by CD5^{hi} DCs than the expansion achieved by CD5^{int} and CD5^{neg} DCs (Fig. 2, F and G). Further, the frequencies of CD8$^+$ T cells that produced IFN-γ (Fig. 2, G and H), as well as the frequencies of the effector molecules granzyme B and perforin (Fig. 2I), were higher after priming by CD5^{hi} DCs than the frequencies detected after priming by CD5^{int} and CD5^{neg} DCs (35.3 versus 20.5 versus 17.9%, respectively, for IFN-γ; 25.3 versus 12 versus 5.29%, respectively, for granzyme B and perforin).

We have previously defined three major subpopulations (monocytotoxic, dicytotoxic, and tricytotoxic) of CTLs (*10*); therefore, we also monitored the frequency of multifunctional CTLs primed by CD5^{hi}, CD5^{int}, and CD5^{neg} DCs. Monocytotoxic T lymphocytes (M-CTLs) express only a single effector molecule (granzyme B, perforin, or granulysin), whereas dicytotoxic T lymphocytes (D-CTLs) express such effector molecules in pairs and tricytotoxic T lymphocytes (T-CTLs) express all three molecules. CD5^{hi} DCs primed a higher frequency of T-CTLs and D-CTLs than CD5^{int} and CD5^{neg} DCs (Fig. 2J; 85.5 versus 76.6 and 64.8%, respectively). Similar to the effect on CD8$^+$ T cells, CD5^{hi} DCs promoted substantially greater CD4$^+$ T cell proliferation (Fig. 2K) and IFN-γ production (Fig. 2L) than CD5^{int} and CD5^{neg} DCs.

Next, we used an anti-CD5 mAb reported to block the immunogenicity of CD5 in a soluble state (*30*) to assess the importance of CD5 in inducing T cell activation. Indeed, the presence of this anti-CD5 mAb reduced the proliferation of both CD8$^+$ (Fig. 2M, left) and CD4$^+$ (Fig. 2M, right) T cells, as well as cytokine secretion in the culture supernatant (Fig. 2N). This effect was substantial in CD5$^+$ DC:T cell cocultures, which suggests a key role for CD5 on DCs in their interaction with T cells.

CD5 expression on human DCs directly enhances T cell priming

To assess the contribution of CD5 expressed on DCs to T cell priming, we used a CRISPR gene activation approach (CRISPRa) to up-regulate CD5 expression on CD5$^-$ DCs (*43*). CD5$^-$ DCs were nucleofected with single guide RNAs (sgRNAs) that target the CD5 promoter and dCas9-VP64-p65-Rta (VPR) mRNA or dCas9-VPR mRNA alone. We obtained a marked up-regulation of CD5 expression (CD5_CRISPRa DCs; 77%) on DCs compared with control cells as early as 24 hours after nucleofection (Fig. 3, A and B). This expression was sustained on a subset of cells for 2 days and then declined (Fig. 3B). CD5 up-regulation was not associated with up-regulation of costimulatory molecules CD72, CD40, CD70, CD80, or CD155, as detected by RNA-seq (Fig. 3C) and flow cytometry (Fig. 3D).

Next, we assessed the impact of CD5_CRISPRa on allogeneic naïve T cell priming (Fig. 3E). Carboxyfluorescein succinimidyl ester (CFSE) dilution analysis showed that CD5_CRISPRa DCs induced an increase in T cell proliferation (Fig. 3F) and primed higher numbers of T cells that produce IFN-γ and TNF-α than control DCs, as determined by intracellular staining (Fig. 3G). CD5 expression on DCs also led to increases in IFN-γ (Fig. 3H) and the T_H2 cell cytokine IL-13 in the culture supernatants (Fig. 3I).

To determine the impact of CD5 on T cell activation by other types of DCs, we induced monocytes to differentiate into DCs (moDCs) by incubation with granulocyte-macrophage colony stimulating factor (GM-CSF) and IL-4 for 5 days. Similar to dermal CD14$^+$ DCs, which

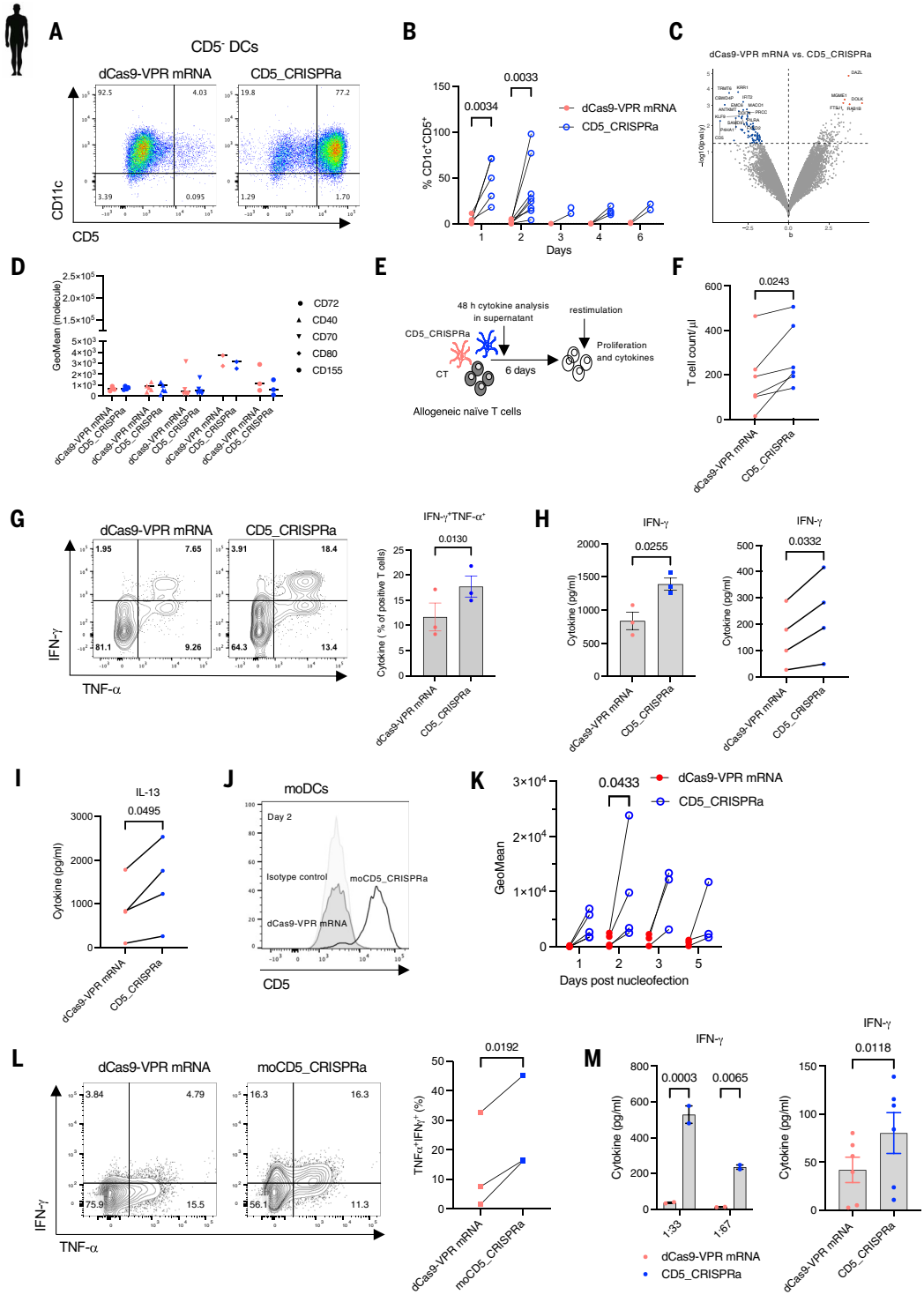

Fig. 3. Up-regulation of CD5 on human DCs promotes effector T cell activation. (**A**) Flow cytometric analysis of CD5 expression in CD5⁻ dermal DCs 48 hours after nucleoporation with or without dCas9-VPR mRNA and sgRNAs. One representative plot of eight experiments is shown. (**B**) Flow cytometric analysis of CD5 expression on dermal CD5⁻ DCs 1 to 6 days after nucleoporation with dCas9-VPR mRNA and CD5a sgRNAs or control dCas9-VPR. Symbols indicate values from individual donors. Composite data of CD5 expression analyzed 1 day (n = 7 donors), 2 days (n = 8 donors), 3 days (n = 2 donors), 4 days (n = 4 donors), and 6 days (n = 2 donors) after nucleofection are shown. (**C**) Volcano plot showing differentially expressed genes between control dCas9-VPR mRNA–electroporated CD5⁻ DCs and CD5_CRISPRa DCs. Genes up-regulated and down-regulated in CD5_CRISPRa DCs are shown in blue and red, respectively. (**D**) Flow cytometric analysis of the expression of CD72, CD40, CD70, CD80, and CD155 by control dCas9-VPR mRNA–electroporated CD5⁻ DCs and CD5_CRISPRa DCs 24 hours after nucleofection. Composite data of at least four donors analyzed for each marker are shown. (**E**) Workflow used in (F) to (I). CT, control. (**F**) Numbers of T cells with diluted CFSE (one division or more) as analyzed on day 6 of the coculture. Composite data of four performed experiments with five donors are shown. (**G**) CD5_CRISPRa or dCas9-VPR mRNA CT dermal DCs were cultured for 6 days with allogeneic naïve CD4⁺ and

$CD8^+$ T cells. Percentages of IFN-γ– and TNF-α–expressing T cells were determined by flow cytometry 6 hours after activation. One representative experiment out of three performed is shown (left). The graph shows composite data of three independent experiments; data represent means ± SEM (right). (**H**) IFN-γ production by T cells after activation for 48 hours with CD5_CRISPRa Langerhans cells or dCas9-VPR mRNA. One representative experiment of five performed with five different donors is shown. Data represent means ± SEM (n = 3) (left). Composite data of four additional experiments performed in the same way using CD5_CRISPRa dermal DCs or dCas9-VPR mRNA CT DCs (right). (**I**) T helper cytokine (IL-13) production after activation of T cells for 48 hours with CD5_CRISPRa or dCas9-VPR mRNA. The graph shows composite data of four independent experiments. (**J**) CD5 expression in moDCs 2 days after nucleoporation with or without dCas9-VPR mRNA and sgRNAs. One representative experiment of five performed with five donors is shown. (**K**) Composite data of CD5 expression analyzed 1 day (n = 5 donors), 2 days (n = 4 donors), 3 days (n = 3 donors), and 5 days (n = 3 donors) after nucleofection are shown. (**L**) Frequency of IFN-γ– and TNF-α–expressing T cells after 6 days of activation with CD5_CRISPRa or dCas9-VPR mRNA moDCs. One representative experiment of three performed is shown. Data represent means ± SEM (left). Composite data of three experiments performed with three different donors are shown (right). (**M**) IFN-γ production that was measured in the culture supernatant of naïve T cells after 2 days of activation with CD5_CRISPRa or dCas9-VPR mRNA moDCs at a T:DC ratio of 33:1 or 67:1. One representative experiment is shown. Data represent means ± SEM (left). Composite data of three additional experiments performed at a T:DC ratio of 40:1 in duplicates or triplicates with three different donors are shown (right). In (B), (F) to (I), and (K) to (M), the numbers over the brackets are P values.

are of monocytic origin, these cells do not express CD5 (*18*). We then induced CD5 expression by moDCs using CRISPRa and evaluated the stability of its expression on the cell surface by flow cytometry. The highest CD5 expression was detected on day 2 (Fig. 3, J and K). CD5 was reduced on day 3 and was further reduced by day 5 (Fig. 3K). Similar to the results obtained with skin DCs, CD5_CRISPRa moDCs induced higher naïve allogeneic T cell activation than nonactivated moDCs, which was indicated by the production of IFN-γ and TNF-α, as detected by intracellular staining (Fig. 3L) and in the culture supernatant (Fig. 3M). Moreover, CD5_CRISPRa moDCs were ~1.6 times more efficient than control moDCs at prompting reactivation of autologous effector Flu-M1–specific $CD8^+$ T cells, as measured by the binding of a specific MHC tetramer (fig. S5, A and B). Overall, our data indicate that CD5 on DCs functions to activate effector T cell responses.

CD5 is functional on mouse DCs

We verified earlier studies in mice (*15*, *22*, *24*) showing that CD5 is expressed on splenic and LN DCs (fig. S6A) and further identified them particularly on resident LN DCs (fig. S6, B and C). In contrast to human DCs, CD5 was not restricted to a certain DC lineage in mice but was instead detected on the two conventional DC subsets: cDC1 ($CD24^+XCR1^+$) and cDC2 (shown as CD172a/SIRP-α^+CD24^-) (fig. S6, D to F). To gain a better understanding of the intrinsic roles of CD5 on DCs in pathological conditions in vivo, we generated conditional CD5 knockout (KO) mice using CRISPR-Cas9 technology to delete CD5 specifically in DCs [CD5ΔDC; fig. S6, A, E, and F, and (*44*)]. Compared with DCs, T cells expressed higher levels of CD5, and the T cells' CD5 expression remained high in the CD5ΔDC mice, in which *Cd5* is deleted under the control of the *Zbtb46* promotor (fig. S6, A, G, and H). This was in contrast with the *Cd11c* (*Itgax*)–Cre line, which was not specific for DCs and led to CD5 deletion in 50% of T cells (fig. S6H). Quantification of the number of CD5 molecules on the surface of the DCs revealed higher expression of CD5 on cDC2 than cDC1 (fig. S6I). Deletion of CD5 on DCs in CD5ΔDC mice was not complete relative to mice with global deletions in CD5 (CD5KO mice) (fig. S6, J and K) but was greater than in mice missing one allele of CD5 (heterogeneous) (fig. S6L). We did not detect differences in gene expression in cDC1 or cDC2 isolated from CD5ΔDC mice versus control mice (fig. S6M), particularly related to immune checkpoint proteins such as CD86, CD40, and programmed cell death ligand 1 (PD-L1) (fig. S6N). The numbers of DCs (including cDC1, cDC2, and plasmacytoid DCs) and T cells ($CD8^+$ or $CD4^+$ T cells) in CD5ΔDC mice were also comparable to those in control mice in both spleens and LNs (fig. S6O).

To evaluate the potential requirement for expression of CD5 by DCs to mount immune responses to tumors in vivo, we adopted a mouse model of tumor generation using a modified 3-methylcholanthrene (MCA)–induced syngeneic sarcoma cell line (MCA1956) that expresses membrane-associated ovalbumin (OVA) (MCA1956-mOVA) (*45*) (Fig. 4A). In this model, tumor elimination is dependent on antigen presentation by DCs through the expression of mOVA that converts MCA1956 tumors into regressor tumors. Tumor elimination was observed in 14 out of 15 wild-type (WT) (control) mice (Fig. 4, B and C). By contrast, CD5ΔDC mice (9 out of 11) failed to reject mOVA tumors, thus confirming a requirement for CD5 expression by DCs for tumor rejection (Fig. 4, B and C). Of note, a single copy of CD5 was sufficient to induce tumor rejection (Fig. 4C). Furthermore, SIINFEKL-H-$2K^b$ tetramer$^+$ $CD8^+$ T cells expanded in control mice in response to MCA1956-mOVA but were reduced in CD5ΔDC mice (Fig. 4D). Overall, our data indicate that CD5 on DCs functions to activate antitumor effector $CD8^+$ T cell responses.

CD5 expression on DCs is required for de novo priming of $CD5^{hi}CD4^+$ conventional T cells by DCs

To determine whether CD5 on DCs also regulates $CD4^+$ T cell responses, we performed antigen-specific T cell activation assays by culturing CD5-deficient DCs (from CD5ΔDC mice or CD5KO mice) or control cDC2s with purified T cells from OT-II mice (Fig. 4E) in the presence of a long peptide containing the MHC II–restricted epitope. We determined the level of T cell proliferation and activation based on CFSE dilution and CD44 expression. After loading with antigenic peptide, CD5-deficient cDC2s from CD5ΔDC mice were less efficient at activating $CD4^+$ OT-II T cells than controls (Fig. 4E). In addition, consistent with the greater deletion of CD5 in CD5KO DCs, the proliferation and activation of OT-II T cells was lower than that of the CD5ΔDC2s for all tested peptide concentrations (Fig. 4E). Moreover, the amount of CD5 on the proliferating T cells correlated with the expression on the DCs (Fig. 4F); that is, control DC-activated T cells expressed higher amounts of CD5 compared with those activated by CD5-deficient DCs (CD5ΔDC or CD5KO).

To confirm these findings in vivo, we investigated the potential requirement for CD5 on DCs for the priming of $CD5^{hi}CD4^+$ conventional T cells. We examined early $CD4^+$ T cell proliferation in response to OVA synthetic long peptide (SLP) vaccine by transferring OVA-specific OT-II transgenic CD4 T cells into control or CD5ΔDC mice (Fig. 4G). OT-II cells underwent cell division in the spleen of control mice, consistent with recognition of $OVA_{323–339}$ peptide–MHC II complexes on DCs, and the proliferating cells expressed high levels of CD5 [Fig. 4, H and I (blue)]. By contrast, CD5 expression on proliferating OT-II cells was markedly reduced in CD5ΔDC mice wherein the CD5 expression on DCs is targeted for deletion and was absent on OT-II cells activated in CD5KO mice, which are characterized by complete deletion of CD5 [Fig. 4I (red and black)]. Overall, these data show that CD5 levels on DCs have a direct impact on CD5 expression on primed T cells.

Optimal benefit of ICB therapy requires $CD5^+$ DCs

We next evaluated the potential requirement for CD5 expression by DCs to mount immune responses to tumors in vivo using mouse tumor models that are dependent on DCs for tumor elimination by ICB therapy (Fig. 4J). We first analyzed responses to MCA1956 tumors

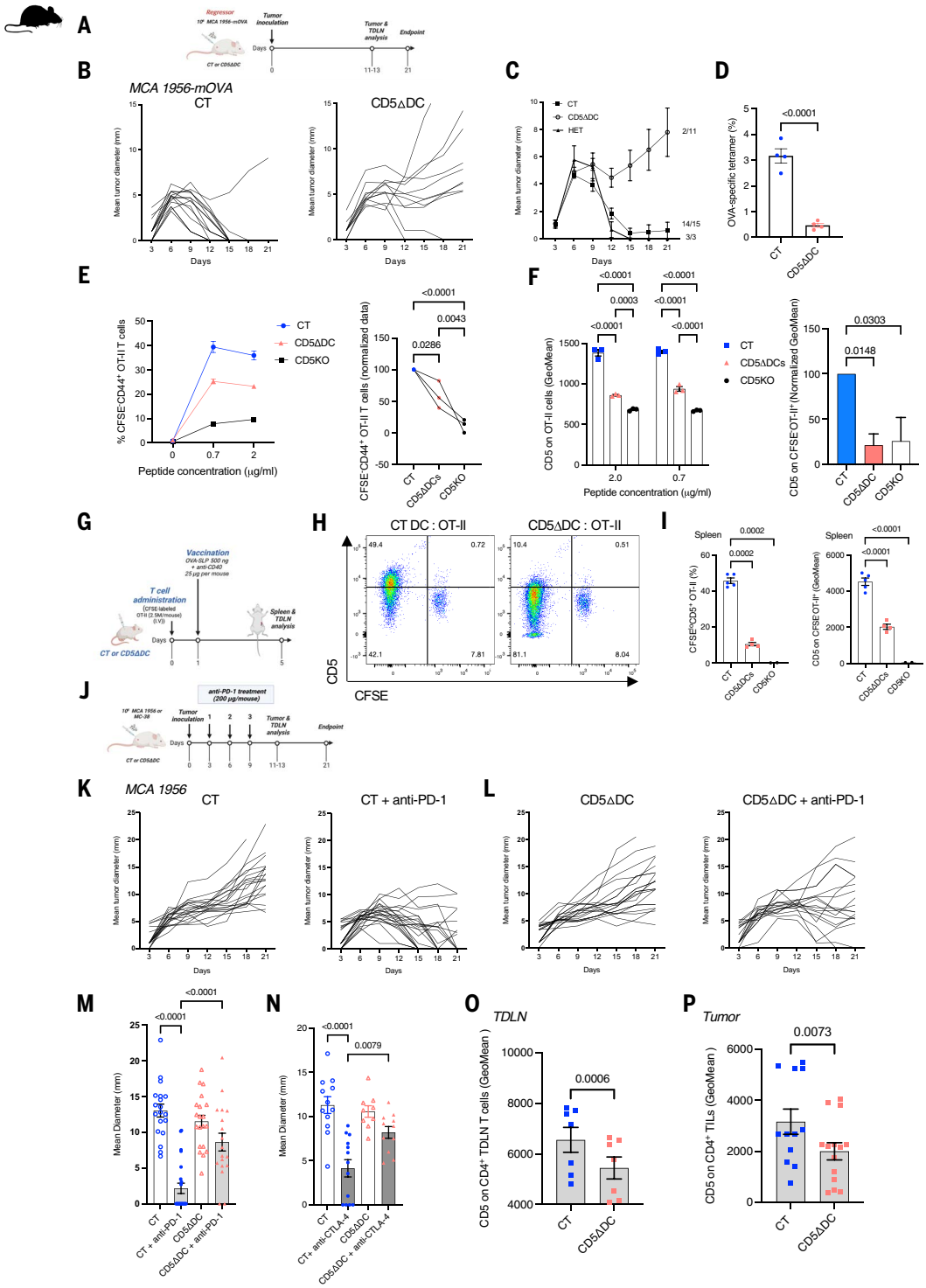

Fig. 4. Deletion of CD5 on DCs compromises the response to ICB therapy and modulates T cell immunity in vivo. (**A**) Workflow of MCA1956-mOVA tumor growth in WT control (CT) or CD5ΔDC mice. (**B**) MCA1956-mOVA tumor growth in CT or CD5ΔDC mice. Results depict tumor growth curves of individual mice from three pooled experiments: CT (WT) (n =15) and CD5ΔDC (n = 11). (**C**) MCA1956-mOVA tumor growth in CT, CD5ΔDC, or $CD5^{HET}$ heterozygous (HET) mice. Combined tumor growth curves for CT (n = 15), CD5ΔDC (n = 11), and HET (n = 3) mice are shown. Overall group difference average as measured across time for CD5ΔDC versus CT (P = 0.0055) and CD5ΔDC versus HET (P = 0.0087). There was no difference between HET and CT. Data represent means ± SEM. (**D**) Binding of OVA:I-A^d tetramer to TDLN cells isolated from MCA1956-mOVA–bearing CT and CD5ΔDC mice. Data represent means ± SEM (n = 4). (**E**) In vitro OT-II cell proliferation in response to cDC2s isolated from CT, CD5ΔDC, and CD5KO mice and cultured with SLP from the OVA protein (OVA-SLP) that contains the MHC II–restricted peptide. One representative experiment of three is shown. The plot shows means ± SEM of three experimental replicates (left). Proliferated OT-II cells in response to cDC2s loaded with 0.7 μg/ml SLP. The mean of three pooled experiments is displayed with normalization to the control (right). (**F**) CD5 mean expression on OT-II cells proliferating in response to cDC2s isolated from CT, CD5ΔDC, or CD5KO DCs (left). Data represent means ± SEM

of three pooled experiments displayed with normalization to the control (right). (**G**) Workflow of OVA-SLP vaccination and analysis of the immune response. (**H**) Representative plot showing CD5 expression on proliferating OT-II T cells in CT or CD5ΔDC mice in vivo. (**I**) Frequency of proliferating $CD5^+OT\text{-}II^+$ cells isolated from the spleen of CT (n = 5), CD5ΔDC (n = 4), or CD5KO (n = 2) mice (left). Mean CD5 expression on proliferating OT-II T cells in CT (n = 5), CD5ΔDC (n = 4), or CD5KO (n = 2) mice in response to SLP vaccine in vivo (right). (**J**) Workflow of the analysis of immune cell infiltration of MCA1956 tumors in mice treated with anti–PD-1 or IgG2a isotype control. Part of the illustration was created with Biorender.com. (**K**) Tumor growth from CT mice injected with immunoglobulin G2a (IgG2a) isotype control or anti–PD-1 antibodies (18 to 23 mice per group). Data represent the results of four pooled experiments. (**L**) Tumor growth from CD5ΔDC mice injected with IgG2a isotype control or anti–PD-1 antibodies (18 to 23 mice per group). Data represent the results of four pooled experiments. (**M**) Mean tumor diameter in CT or CD5ΔDC mice on day 21 after implantation and treatment with IgG2a isotype control or anti–PD-1 antibodies. Data represent the results of four pooled experiments. (**N**) Mean tumor diameter in CD5ΔDC and CT mice on day 24 after implantation and treatment with isotype control or anti–CTLA-4 antibodies. (**O**) CD5 expression by $CD4^+$ T cells in the lymphoid immune compartment in the TDLNs of CD5ΔDC or CT mice treated with isotype control or anti–PD-1 antibodies. (**P**) CD5 expression by $CD4^+$ T cells in the lymphoid immune compartment in the tumor of CD5ΔDC or CT mice treated with isotype control or anti–PD-1 antibodies. In (D) to (F), (I), and (M) to (P), the numbers over the brackets are P values. [Illustrations in (A), (G), and (J) created with Biorender.com]

in WT control and CD5ΔDC mice. MCA1956 tumors grew progressively in both control and CD5ΔDC mice [Fig. 4, K (left) and L (left)]. However, whereas control mice responded effectively to anti–PD-1 ICB therapy ($P > 0.0001$) (Fig. 4K, right), CD5ΔDC mice responded less efficiently and the tumor was not rejected (Fig. 4L, right). Whereas 18 out of 23 tumor-bearing control mice responded to anti–PD-1 treatment and 15 out of 23 completely rejected the tumor, only 2 out of 18 CD5ΔDC mice rejected tumors, with an average tumor size at day 21 after anti–PD-1 treatment of 2.1 ± 0.7 mm in control mice compared with 8.6 ± 1.2 mm in CD5ΔDC mice (Fig. 4M). Similar results were obtained using anti–CTLA-4 therapy (Fig. 4N). Compared with control mice, CD5ΔDC responded less efficiently to the treatment. The average tumor size at day 18 after anti–CTLA-4 treatment was 4.1 ± 0.9 mm in control mice compared with 8.2 ± 0.6 mm in CD5ΔDC mice. At this early time point, 5 out of 13 control mice had already rejected the tumors, whereas none of the CD5ΔDC mice showed complete rejection of the tumors (Fig. 4N).

The $CD5^{lo}$ T cell population is expanded in the TME of CD5ΔDC mice

To understand the impact of the absence of CD5 expression on DCs in shaping the T cell milieu in the TME, we examined the immune infiltrates in the tumor and TDLNs of MCA1956-bearing control or CD5ΔDC mice by flow cytometry (Fig. 4, O and P). We found that $CD8^+$ and $CD4^+$ T cells were equally represented in tumor infiltrates from control and CD5ΔDC mice after ICB therapy (fig. S7A), and no difference in regulatory T cell infiltrates was detected (fig. S7B). Although no difference in CD5 expression was observed on $CD4^+$ T cell subsets under steady-state conditions (fig. S7C), CD5 expression on the primed $CD4^+$ T cells in the TDLNs of CD5ΔDC mice was lower than that in the control mice after ICB therapy (5443 ± 436 versus 6555 ± 494). This further emphasizes that CD5 on DCs modulates CD5 expression by $CD4^+$ T cells, which are critical for tumor rejection, during an immune response at the site of activation (Fig. 4O) (*46*).

Reduced CD5 expression on $CD4^+$ T cells was also detected in the tumor infiltrates of CD5ΔDC mice relative to CT mice (2002 ± 337.3 versus 3161 ± 495) (Fig. 4P). CD5 expression on the $CD4^+$ T cells in the tumor was lower than that detected in the TDLNs (3161 ± 495 versus 6555 ± 494) [Fig. 4, O and P (blue)]. For control tumor-infiltrating lymphocytes, CD5 expression on the $CD8^+$ T cells was lower than that on the $CD4^+$ T cells (1851 ± 302 versus 3161 ± 495), with no difference in CD5 expression on $CD8^+$ T cells in control mice compared with that of the corresponding population in CD5ΔDC mice (fig. S7, D and E). Anti-CD3 induced CD5 up-regulation in T cells that were isolated from CD5ΔDC mice, which confirmed that the priming of $CD5^{lo}$ T cells was directly affected by CD5-deficient DCs (fig. S7F). Anti–PD-1 or anti–CTLA-4 alone did not modulate CD5 expression on T cells (fig. S7F), supporting the requirement for T cell receptor (TCR) stimulation by DCs. Additionally, the frequency of inducible T cell costimulator $(ICOS)^+CD4^+$ T cells was reduced in tumor infiltrates of CD5ΔDC mice compared with those of control mice (fig. S7G, left). By contrast, a higher frequency of T cell immunoreceptor with immunoglobulin and immunoreceptor tyrosine-based inhibitory motif domains $(TIGIT)^+CD4$ T cells was found in the tumors of CD5ΔDC mice after anti–PD-1 treatment (fig. S7G, right). The frequency of activated (fig. S7H, left) and granzyme B–expressing $CD8^+$ T cells was also reduced in tumor infiltrates of CD5ΔDC mice (fig. S7G, right).

We next used the MC-38 colorectal cancer model to determine the effect of the deletion of CD5 expression by DCs in the priming of tumor-specific $CD8^+$ T cells. Neoantigen-specific $CD8^+$ T cells that are reactive against the mutated epitopes from the adenosine diphosphate (ADP)–specific glucokinase (ADPGK) proteins were detected in control tumors. However, the frequency of these antigen-specific $CD8^+$ T cells was reduced in tumors from CD5ΔDC mice (fig. S8, A and B). Moreover, CD5 expression on the antigen-specific T cells was lower after priming by CD5ΔDCs relative to that of cells primed by control DCs (fig. S8C). Overall, these data show that deletion of CD5 expression on DCs favors the expansion of $CD5^{lo}$ T cells and the reduction of tumor-specific $CD8^+$ T cells.

CD5 deletion on T cells dampens tumor elimination in response to ICB therapy

To address the impact of low CD5 expression by T cells in restraining tumor rejection in CD5ΔDC mice, we developed mice with CD5-deficient T cells by crossing $Cd5^{flox/flox}$ ($Cd5^{f/f}$) mice with $Cd4^{cre+}$ mice (CD5ΔT) (fig. S9, A and B). In these animals, CD5 expression is maintained on DCs but is deleted in both $CD4^+$ and $CD8^+$ T cells (fig. S9, C and D). There was no significant difference in the frequency of T cells (fig. S9E) or DC frequency (fig. S9F) in CD5ΔT mice compared with control mice or in the expression of CD3, activating (ICOS), or inhibitory (PD-1) molecules (fig. S9G). MCA1956 tumor growth was comparable in control and CD5ΔT mice (Fig. 5, A and B). However, whereas the majority of the control mice (13 out of 16) responded to anti-PD1 treatment, with eight completely rejecting the tumor, none of the CD5ΔT mice (0 out of 14) responded to the treatment (Fig. 5, C and D). Furthermore, CD5ΔT mice (25 out of 27) failed to reject MCA1956-mOVA cells, which were rejected spontaneously in control mice (Fig. 5E; $P < 0.0001$). This was also reflected by the reduced frequencies of OVA-positive $CD8^+$ T cells in the tumor (Fig. 5F, left) and spleen (Fig. 5F, right) of CD5ΔT mice. This result was not restricted to the MCA1956 tumor because the failed tumor rejection by CD5ΔT mice in response to anti–PD-1 treatment was also observed in the murine MC-38, adenocarcinoma of the colon, tumor model (fig. S10). Control mice efficiently rejected the tumor in response to anti–PD-1 treatment (P = 0.0007); however, CD5ΔT mice failed to respond (fig. S10A), which correlated with reduced frequencies of tetramer-positive $CD8^+$ T cells specific for the neoantigens ADPGK and RALBP1 associated Eps domain containing 1 (REPS1) in the tumor (fig. S10, B and C). Collectively, these data suggest that high CD5 expression on T cells facilitates the control of tumor growth in response to ICB therapy.

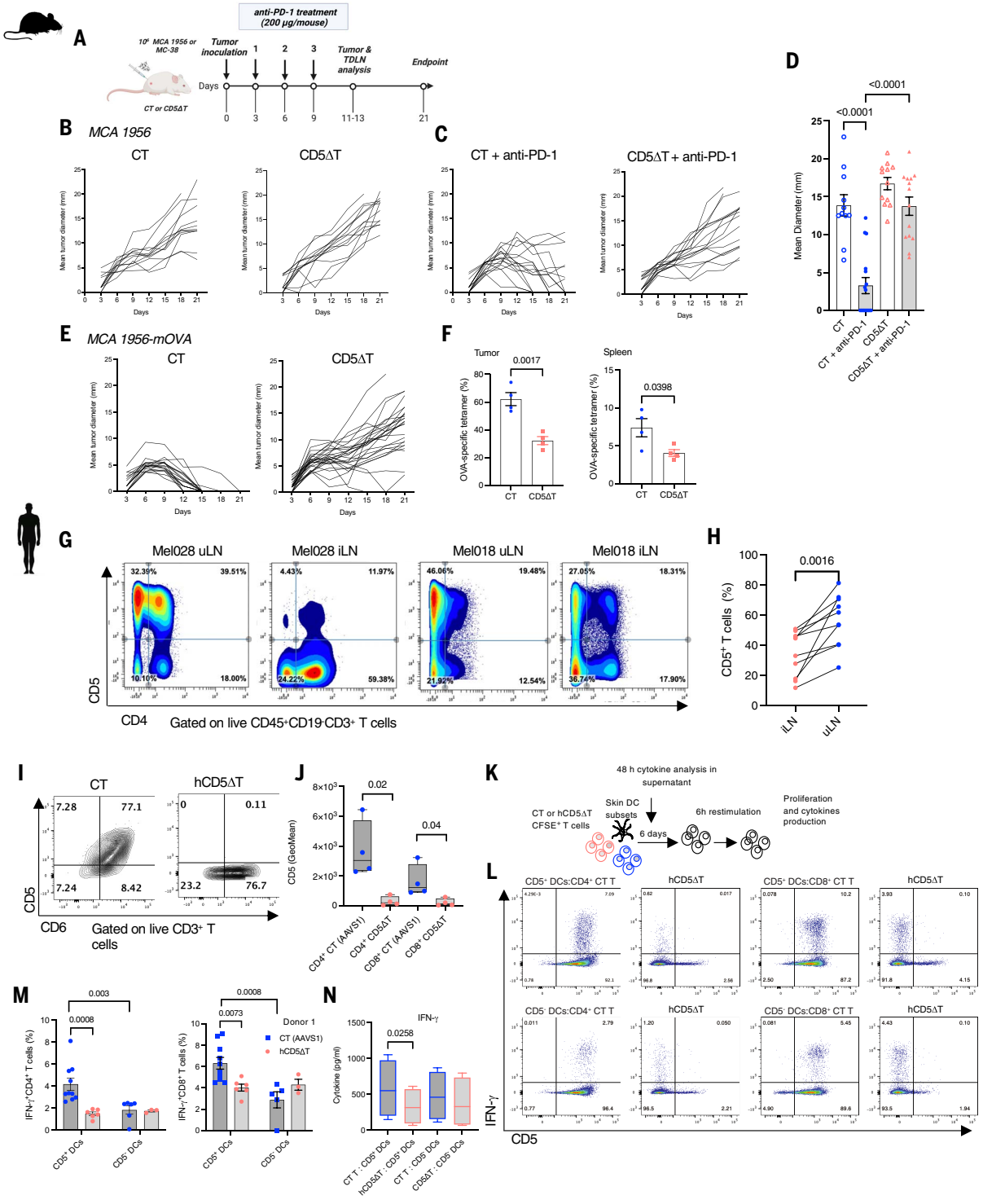

Fig. 5. Deletion of CD5 on T cells compromises effector T cell priming and response to ICB therapy. (**A**) Workflow of tumor growth in control (CT) or CD5ΔT mice. MCA1956 tumor growth in CT (WT) or CD5ΔT mice injected with IgG2a isotype control or anti–PD-1 antibodies. [Illustration created with Biorender.com] (**B**) Results depict tumor growth curves of individual mice from three pooled experiments for CT (n = 12) and CD5ΔT (n = 13). (**C**) Results depict tumor growth curves of individual mice from three pooled experiments for CT with anti–PD-1 (n = 13) and CD5ΔT with anti–PD-1 (n = 16). Overall group difference as measured across time for CD5ΔT versus CT (P < 0.0001). (**D**) Average tumor growth on day 21 in CT or CD5ΔT mice treated with anti–PD-1 or isotype control IgG2a. Data represent means ± SEM. (**E**) MCA1956-mOVA tumor growth in CT or CD5ΔT mice. Results depict tumor growth curves of individual mice from three pooled experiments for CT (n = 15) and CD5ΔT (n = 8). Overall group difference as measured across time for CD5ΔT versus CT (P < 0.0001). (**F**) Frequency of OVA-specific $CD8^+$ T cells that were detected in the tumor (left) and spleen (right) of CT and CD5ΔT mice 10 days after tumor cell inoculation. Data represent means ± SEM. (**G**) Expression of CD5 on T cells (gated on live, $CD45^+CD19^-CD3^+$; plots show CD4 expression versus CD5 expression) in iLNs and uLNs of two representative patients, Mel028 and Mel018. (**H**) Composite data showing the frequency of $CD5^+$ T cells in iLNs and uLNs of 10 patients with melanoma. Data represent means ± SEM. (**I**) CD5 and CD6

expression on CT or hCD5ΔT cells after coculture with DCs. (**J**) CD5 geometric mean expression on CT or hCD5ΔT CD4$^+$ or CD8$^+$ T cells before coculture with DCs. Composite data of four donors are shown. Data represent means ± SEM. (**K**) Experimental scheme for (L) to (N). (**L**) Frequency of IFN-γ expression by CD4$^+$ and CD8$^+$ T cells in CT or hCD5ΔT cultures with CD5$^+$ or CD5$^-$ dermal DCs. Data represent one experiment of four performed. (**M**) Flow cytometric frequency analysis of IFN-γ expressed by CT or hCD5ΔT CD4$^+$ (left) or CD8$^+$ (right) T cells cocultured with either CD5$^+$ or CD5$^-$ DCs. Data represent one experiment of four performed with four different donors (see also fig. S11E). Each dot indicates a technical replicate. Data represent means ± SEM. (**N**) IFN-γ production measured in the culture supernatant of either CT T cells or hCD5ΔT cells cocultured with either CD5$^+$ or CD5$^-$ DCs. Composite data of four experiments performed with four donors are shown. Data represent means ± SEM. In (D), (F), (H), (J), (M), and (N), the numbers over the brackets are *P* values.

CD5 deletion on human T cells mirrors CD5 deletion on DCs

To determine the correlation between CD5$^+$ DC density and CD5 levels on T cells in human tumors, we assessed the expression of CD5 on T cells in iLNs and patient-matched uLNs by CyTOF. We found that a larger fraction of T cells (both CD4$^+$ and CD8$^+$ T cells) in the uLNs expressed CD5 and that this proportion was reduced in the corresponding metastatic tumor LNs (Fig. 5, G and H). To determine the functional requirement for CD5 expression on human T cells, we designed an sgRNA for *CD5* disruption in primary human T cells using a nonviral CRISPR-Cas9–based protocol (*47*). We confirmed the gene deletion efficiency by insertion-deletion (indel) analysis (fig. S11A) and flow cytometry (Fig. 5I and fig. S11B). CD5 disruption was effective in both CD4$^+$ and CD8$^+$ T cells (Fig. 5J and fig. S11B). Similar to mice, the expression of CD5 was higher on CD4$^+$ T cells than on CD8$^+$ T cells (Fig. 5J and figs. S9A and S11B). CD6, the expression of which parallels CD5 expression in T cells (*48*, *49*), was not affected in the human CD5-deleted T cells (hCD5ΔT) (Fig. 5I and fig. S11C). In addition, there was no substantial difference in the expression of activating and inhibitory receptors, including CD69, PD-1, CCR7, and CD25 (fig. S11, C and D, and table S3). We then stimulated unedited control T cells or hCD5ΔT cells with CD5$^-$ or CD5$^+$ DCs and measured the production of effector cytokines (Fig. 5, K to N, and fig. S11, E and F). Compared with the control cells, hCD5ΔT cells (both CD4$^+$ and CD8$^+$) produced lower amounts of IFN-γ. Indeed, CD5 expression on T cells was important for T cell activation but was inhibited when CD5 was also expressed by the primed DCs, indicating a critical role for CD5 on DCs in the interaction of CD5 on T cells (Fig. 5, L to N, and fig. S11, E and F). This was determined by the amounts of cytokines detected by intracellular staining of IFN-γ in CD4$^+$ (Fig. 5M, left) and CD8$^+$ T cells (Fig. 5M, right, and fig. S11E) and in the culture supernatant amounts of IFN-γ and IL-5 (Fig. 5N and fig. S11F). Although gene expression analysis of CD5 ligation on T cells indicated no changes in expression (table S4), T cell CD5 potentiated the production of TCR-induced T cell cytokines IFN-γ and TNF-α when cross-linked by two clones of anti-CD5 mAb [#OKT1 (fig. S12A) and Novus #T1 (fig. S12B)] that function as agonists. Overall, these data demonstrate that engagement of CD5 on T cells in concert with TCR stimulation potentiates inflammatory T cell responses, which are a critical component of the response to ICB therapy in patients.

CD5$^+$ DCs are increased in response to ICB therapy

To better understand the mechanism by which CD5$^+$ DCs promoted a favorable response to ICB therapy in control mice, we examined the frequency of CD5$^+$ DCs in the tumors and TDLNs of mice 11 to 13 days after MCA1956 cell inoculation (Fig. 6A). Although the DC (fig. S13A) and macrophage (fig. S13B) frequencies were not altered in response to ICB therapy, such treatment up-regulated the CD5$^+$ DC frequency in both the tumor (Fig. 6B) and the TDLN (Fig. 6C) DC1 and DC2 compartments. This effect of anti–PD-1 was also seen with the MC-38 tumors (fig. S13C). Mechanistically, this effect was likely not due to enhanced migration. CD5$^+$ DCs were mainly found within resident LN DCs (identified by IE/IA^{lo}CD11c^{hi}; fig. S13D, left) and showed lower levels of CCR7 than the CD5$^-$ DCs (fig. S13D, right), albeit its expression was slightly increased after anti–PD-1 treatment, particularly on CD5$^+$ DC1s (fig. S13E). In addition, there was no impact on the CD5$^+$ DC proliferative state after anti–PD-1 treatment, although CD5$^+$ DCs expressed higher levels of K_i-67 than the CD5$^-$ DCs (fig. S13F). Importantly, however, CD5$^+$ DCs were more resistant than CD5$^-$ DCs to apoptosis in vitro (Fig. 6D), and CD5$^+$ DCs, including CD5$^+$ DC1s and CD5$^+$ DC2s but not CD5$^-$ DCs, were ~50% more resistant to apoptosis in the presence of anti–PD-1 in vivo (Fig. 6E and fig. S13G). Overall, these data indicate that CD5$^+$ DCs are targets of immune suppression in the TME, thus implicating the priming of new T cells by CD5$^+$ DCs as a critical step for the efficiency of ICB therapy.

Low levels of IL-6 promote the development of CD5$^+$ DCs

To determine factors that might promote CD5$^+$ DC development and persistence in response to anti–PD-1, we studied the properties of DCs from a patient with inherited PD-1 deficiency. This revealed that a higher proportion of DCs in this patient expressed CD5 compared with control subjects (Fig. 6F) (*50*). We thus hypothesized that this increased frequency of CD5$^+$ DCs might be caused by the excessive IL-6 production in this patient. Moreover, we detected an increase in IL-6 production by immune cells in the TME of mice treated with anti–PD-1 (Fig. 6G). Indeed, the presence of IL-6 during DC differentiation from bone marrow (BM) progenitors favored the development of CD5$^+$ DCs (Fig. 6, H and I). High concentrations of IL-6 (250 ng/ml) skewed the development from DC1 toward DC2 [SIRP-α$^+$; fig. S13H (dark blue)] (*51*, *52*); however, low IL-6 concentrations (below 20 ng/ml) increased the expression of CD5 on both of these DC subsets [Fig. 6, H and I, and S13H (light blue)]. The same pattern was observed in human DCs, with the presence of IL-6 found to promote the differentiation of CD5$^+$ DCs from cord blood CD34$^+$ hematopoietic progenitor cells (HPCs) [Fig. 6, J and K, and fig. S13, I, J (dark blue), and K]. To determine whether IL-6 up-regulates CD5 expression rather than increasing the differentiation of CD5-expressing murine DCs, purified splenic DCs were exposed to IL-6 for 5 days (fig. S13L). Similarly, sorted human dermal CD5$^+$ and CD5$^-$ DCs were exposed to IL-6 (fig. S13M). Under these conditions, CD5 remained on the surface of the positive cells, and its expression did not change on terminally differentiated mouse DCs (fig. S13L) or human DCs [fig. S13M, left (blue)]. Moreover, CD5 expression was not detected on IL-6–stimulated CD5$^-$ DCs [fig. S13M, left (red) and right]. IL-23, which was also abundant in the PD-1–deficient patient, did not affect CD5 expression on CD5$^-$ DCs (fig. S13N) nor did it have any impact on CD5$^+$ DC differentiation from mouse BM progenitors (fig. S13O) or human CD34$^+$ HPCs [fig. S13, J (orange) and P]. Moreover, ligation of CD5 on human DCs with an agonistic mAb (fig. S14, A and B) promoted the production of cytokines and up-regulation of gene pathways related to IL-6 and TNF-α signaling (fig. S14C), as well as other genes associated with DC differentiation [colony-stimulating factor 2 (*CSF2*), *GMCSF*], survival (*BCL2*), and tumor immune cell infiltrate (*SERPINE1*) (*53*, *54*) (fig. S14, D and E, and tables S5 and S6). Thus, low levels of IL-6 promote the differentiation of CD5$^+$ DCs and may further explain the reduced apoptosis and increased frequencies of CD5$^+$ DCs after PD-1 inhibition.

Discussion

In this study, we investigated the mechanisms that underlie DC-mediated effector T cell priming, focusing on the role of CD5 expressed by these interacting cell types. Our results

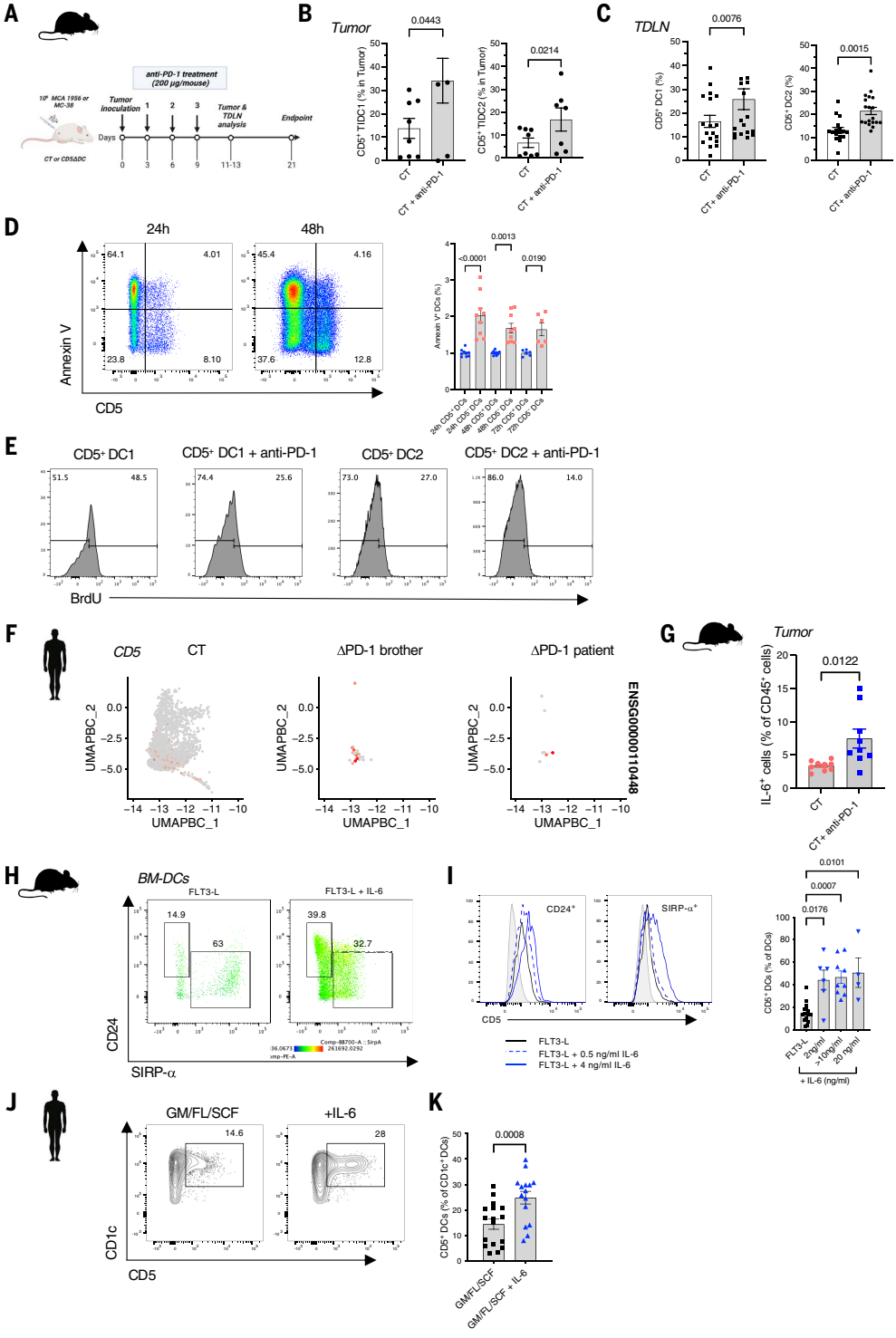

Fig. 6. CD5$^+$ DCs are modulated in the TME. (**A**) Workflow of tumor growth and immune cell infiltrate analysis in control (CT) or CD5ΔDC mice. [Illustration created with Biorender.com] (**B**) CD5 expression of tumor-infiltrating cDC1 (TIDC1) (left) or cDC2 (TIDC2) (right) from CT mice treated with anti–PD-1 (n = 8; three data points are outside the axis limits for TIDC1) or IgG2a isotype control (n = 7). Data represent means ± SEM. (**C**) Frequency of CD5$^+$ cDC1 (left) or CD5$^+$ cDC2 (right) in TDLNs of CT mice treated with IgG2a isotype control (n = 18) or anti–PD-1 antibodies (n = 19). Data represent means ± SEM. (**D**) Plots show the expression of Annexin V by CD5$^+$ and CD5$^-$ splenic DCs after 24 and 48 hours of incubation. One representative experiment is shown. Cells are gated on live, lineage$^-$F4/80$^-$CD64$^-$IE/IA$^+$CD11c$^+$ cells (left). Composite data of three experiments are shown. Each dot represents a different mouse. Annexin V expression was normalized to CD5$^+$ DCs for each indicated time point (right). Data represent means ± SEM. (**E**) CD5$^+$ cDC1s and CD5$^+$ cDC2s isolated from TDLNs of MCA1956 tumor–bearing mice treated with IgG2a isotype control or anti–PD-1 antibodies and stained with an apoptosis detection antibody (APO-BrdU TUNEL assay). Composite data of three mice per group from one of two independent experiments are shown. (**F**) UMAP shows *CD5* gene expression by the myeloid DC clusters isolated from scRNA-seq of the peripheral blood mononuclear cells from a patient with inherited *PD-1* deficiency and the patient's brother, as well as control subjects. The cells were analyzed per the authors'

Mendeley data report [(*50*); see https://data.mendeley.com/datasets/nb26v3mx3x/2]. (**G**) Frequency of IL-6–producing immune cells within tumor-infiltrating immune cells of mice bearing MCA1956 tumors and treated with IgG2a isotype control or anti–PD-1. Data represent means ± SEM (n = 9 mice per group). (**H**) DC1 ($CD24^+$) and DC2 ($Sirp\text{-}\alpha^+$) output from BM cells that were cultured with either Fms-like tyrosine kinase receptor 3 ligand (FLT3-L) or FLT3-L and 4 ng/ml IL-6 for 8 days. CD5 median expression is shown in heatmap statistic plots. (**I**) BM cells were cultured for 8 days with FLT3-L (black line), FLT3-L with 0.5 ng/ml IL-6 (dashed blue line), or FLT3-L with 4 ng/ml IL-6 (solid blue line). CD5 expression on output BM DC1s or DC2s (left) is shown. Composite data showing $CD5^+$ DC output from mouse BM DCs that were cultured with FLT3-L and the indicated amounts (0 to 20 ng/ml) of IL-6; each dot represents an independent experiment (right). Data represent means ± SEM. (**J**) CD5 expression on $CD1c^+$ DCs derived from human $CD34^+$ HPCs that were differentiated with GM-CSF, FLT3-L, and SCF (GM, FL, and SCF) in the presence or absence of IL-6 (100 ng/ml) for 7 days. One experiment is shown. (**K**) $CD5^+$ DC output within the CD34-derived $CD1c^+$ compartments. Cells are gated on live, $lineage^-HLA\text{-}DR^+CD11c^+CD1c^+$. The graph shows composite data of 10 independent experiments. In (B) to (D), (G), (I), and (K), the numbers over the brackets are P values.

demonstrate that CD5 on DCs serves as an immunostimulatory receptor that is important for de novo priming of antitumor T cells and the response to ICB therapy. The amount of CD5 expressed on DCs correlated directly with the extent of effector T cell priming in humans. Selective deletion of CD5 expression by DCs prevented an efficient response to ICB therapy in tumor-bearing mice, which resulted in defective immune rejection of tumors. The cause of this defect was likely that the activation of $CD5^{lo}$ T cells with poor effector function was favored. Similarly, deletion of CD5 expression by T cells negatively affected antitumor immunity and the response to ICB. Importantly, we found increased numbers of $CD5^+$ DCs after ICB in vivo and identified IL-6 as an important factor for $CD5^+$ DC differentiation and survival. Thus, based on our model, we predict that a high density of $CD5^+$ DC2 cells is likely to align with an increased frequency of tumor-specific T cells in patients as well as improvements in $CD5^{hi}$ T cell activity.

We previously identified CD5 on a subset of human $CD1c^+$ DCs (DC2) in migratory skin DCs, peripheral blood, and cord blood. These cells showed a superior capacity to prime T cell responses relative to their $CD5^-$ DC2 counterparts and their numbers were also elevated in inflamed skin (*18*). We hypothesized that in cancer, CD5 expression on DCs has a role in determining the fate of tumor-specific T cells, which renders lymphocytes more capable of efficiently recognizing and eliminating malignant cells. In this study, we indeed found that these cells are present in tumor-free LNs and are reduced in melanoma-affected LNs. Moreover, we showed that CD5 expression, and, specifically, a $CD5^+$ DC signature, are associated with a better prognosis for patients with melanoma, lung squamous cell carcinoma, sarcoma, breast cancer, cervical squamous cell carcinoma, and endocervical adenocarcinoma. CD5 is also an independent prognostic biomarker for overall survival in the early stages of non–small cell lung cancer (*55*). Analysis of TCGA datasets for the statistical significance of T cell–specific *CD5* expression on the overall survival of melanoma patients was not conclusive. This could be due to issues with the analysis or could indicate that the differences in CD5 protein expression do not correspond with the mRNA levels in T cells. Alternatively, the genetic variability of *CD5* might provide an explanation. Single-nucleotide variations s2241002 (C/T; Pro224Leu) and rs2229177 (C/T; Ala471Val) have been associated with severe forms of systemic lupus erythematosus, rheumatoid arthritis, Crohn's disease (*56*), and certain types of cancer (*57*). Furthermore, an inherited functional variant of CD5 influenced melanoma survival (*58*). Thus, different variants might affect $CD5^+$ DC function, interaction with T cells through CD5, signaling, T cell persistence, and, ultimately, patient survival and response to ICB therapy.

The absence of $CD5^+$ DCs in iLNs of patients with melanoma suggests that the TME negatively regulates the differentiation of these DCs from progenitors or, alternatively, reduces their survival. Indeed, we found that CD5 signaling (in humans and mice) enhanced DC survival. Additionally, the treatment of mice with anti–PD-1 increased the frequency of $CD5^+$ DCs in the tumor and lymphoid tissue. Given the apparent irreversibility of certain forms of exhaustion (*59*), it is possible that the efficacy of T cell–targeted immunotherapies is linked to ongoing de novo LN priming by these $CD5^+$ DCs rather than merely a blockade of checkpoint ligands in the tumor. Harnessing the CD5 costimulatory pathway in DCs during priming may increase the efficacy of immunotherapies in conventional T cells. Practically, we envision using these cells for immunotherapy applications. Although we could not identify $CD5^+$ DCs in tonsils, and though they were scarce in human spleen, $CD5^+$ DCs can be efficiently isolated from peripheral blood mononuclear cells and cord blood and can also be differentiated from HPCs (*18*). Moreover, antibodies against CD5 might be used therapeutically to inhibit T cell activation in autoimmunity by blocking their interaction with CD5 on DCs. Indeed, although they may engage CD5 on T cells, we found that antibodies against CD5 could only inhibit T cell activation when CD5 was also expressed by the primed DCs, which suggests that the interaction between CD5 on DCs and T cells is critical for T cell activation.

We help explain the mechanism through which effective ICB therapy alters these signals to favor $CD5^+$ DC differentiation and promote tumor rejection. This mechanism was revealed by investigating the DCs of a patient with inherited PD-1 deficiency (*50*). Such patients, who are susceptible to tuberculosis and autoimmunity, have an immunological profile that mirrors that of patients with signal transducer and activator of transcription 3 (STAT3) gain-of-function disease (*51*) and which is characterized by the production of a large amount of IL-6 by their T cells. In addition, we found that a large proportion of the DCs from one of these patients expressed CD5. Thus, we hypothesized that IL-6 plays a role in $CD5^+$ DC differentiation or survival. Indeed, we identified IL-6 as a factor that drives the differentiation of $CD5^+$ DCs and that could explain the reduced apoptosis of these cells after ICB. It appears that CD5 is induced early on during the differentiation of $CD1c^+$ DCs from $CD34^+$ HPCs (via the $CD14^+CD1c^+$ DC transitioning stage). Moreover, ligating CD5 with an agonistic mAb promoted the production of IL-6 from DCs, which can maintain high expression of CD5 through an autocrine mechanism, thereby inducing de novo differentiation of $CD5^+$ DCs or promoting their survival. CD5 expression by DCs is sensitive to low levels of IL-6, which is expressed in immune cells after ICB therapy. Indeed, we found that low levels of IL-6 were sufficient to promote CD5 expression on DCs without skewing their differentiation toward DC2 or macrophage lineages. Whether other factors could also regulate or promote $CD5^+$ DC differentiation from hematopoietic progenitors or monocytes, as well as the immune cell–specific source of IL-6 during ICB in vivo, remains to be established.

Based on studies performed primarily with murine T cells, CD5 was posited as a negative regulator of T cell function (*27*, *28*, *60*). However, emerging studies indicate its ability to induce T cell activation and pathogenic T_H17 cell differentiation (*34*, *35*). Thus, the functional relevance of CD5 expression on cells remains unresolved and may vary with cell type or microenvironment (*36*, *37*). CD5 expression by DCs was recognized in humans (*18*, *19*) only recently, although it was previously reported in mice (*15*, *22*–*24*). A study by Li *et al.* proposed that CD5 expression by DCs may be correlated with decreased effector T cell

activation and proinflammatory cytokine production (29) and a reduced antitumor response. Multiple factors may explain this discordance with our findings. The study by Li *et al.* mainly used transferred BM-derived DCs (BM-DCs) from CD5KO and control mice to drive their conclusion. The transferred cell subset composition may not be similar between CD5KO and control BM-DCs. In addition, the authors used a Toll-like receptor 4 (TLR4) agonist to trigger cell cytokine production; however, in such CD5-independent DC activation, the expression of this TLR4 on CD5KO and CT DCs may differ. As our data indicate, $CD5^-$ DCs are more sensitive to apoptosis than their $CD5^+$ DC counterparts; therefore, increased cell death of CD5KO DCs may lead to increased inflammation, antigen uptake, and activation of resident WT DCs (61). Further, an enhanced transfer of peptide or peptide-MHC complex (62, 63) from migratory DCs to LN resident DCs in the recipient mice might occur in these types of experiments and may explain the observed increase in T cell proliferation.

Here, we show that CD5 deletion on DCs leads to the priming and activation of $CD5^{lo}$ $CD4^+$ T cells in vivo. CD5 expression on the T cells did not correlate directly with proliferation, as indicated by the dilution of CFSE dye, but was rather affected by the CD5 signal provided by the DCs. In addition to studies in which CD5 was identified as a marker of T cell activation (27, 64), studies using polyclonal and TCR transgenic T cells showed that mature T cell effector functions and memory responses correlate with CD5 expression (65–68). Indeed, T cells that emerge from the thymus with a higher affinity for self-antigens (expressing high levels of CD5; $CD5^{hi}$) also have an increased affinity for a foreign antigen, with a distinct advantage in becoming engaged in both homeostatic and antigen-mediated responses compared with their $CD5^{lo}$ counterparts (66, 69). Moreover, the gene expression profiles of $CD5^{hi}$ and $CD5^{lo}$ naïve T cells suggest that $CD5^{hi}$ cells are transcriptionally poised to engage in both proliferative and effector functions far more rapidly than $CD5^{lo}$ cells of the same specificity (67, 70). CD5 expression is reduced on tolerized cells relative to effector T cells (71), and T cells isolated from the infiltrate of human lung carcinoma patient tumors have lower CD5 expression than T cells with the same antigen reactivity that are isolated from the peripheral blood of the same subject. Our analysis of T cells isolated from melanoma iLNs and uLNs reveals that a higher fraction of CD5-expressing T cells is confined to the uninvolved tissue. Based on our results, it can be speculated that the response to immunotherapy might be less efficient in these patients compared with those exhibiting mixed CD5 expression levels on their tumor-infiltrating lymphocytes (72).

To understand the functional impact of CD5 on T cell responses in vivo, we developed a mouse model in which CD5 expression is controlled in a cell type–specific manner. To delete CD5 in DCs, we used the *Zbtb46*-Cre line because of its high specificity for DCs and DC progenitors (73). By contrast, the *Cd11c (itgax)*–Cre line, which is not specific for DCs, resulted in CD5 deletion in 50% of T cells. The caveat of the *Zbtb46*-Cre line, however, is that one *Cd5* allele is deleted in all progeny. Nevertheless, in spite of the deleted copy in $Zbtb46^{cre+}Cd5^{f/-}$ (CD5ΔDC) mice, the CD5 expression on the T cells was comparable with that of control mice ($Cd5^{f/f}$ or WT), and CD5 expression on DCs was reduced as expected. The expression of *Zbtb46* in DC progenitors might explain the transient *Cre* expression in the germline.

The inhibition of tumor immunity was more pronounced upon deletion of CD5 when using a *Cd4*-Cre line compared with the *Zbtb46*-Cre line. This effect might be due to the complete deletion of CD5 obtained using this line as opposed to the partial deletion seen with the *Zbtb46*-Cre line. Alternatively, there might be an additive effect due to the reduction in CD5 on some DCs in addition to the deletion in T cells in the *Cd4*-Cre line. Indeed, we noted that DCs were affected in this model (because of their expression of *Cd4*) and saw some reduction in CD5 expression on the DCs, particularly in LN DCs.

The extracellular domain of CD5 consists of three subdomains that belong to the scavenger receptor cysteine-rich superfamily. The bona fide ligand or ligands for CD5 remain uncertain but may include the C-type lectin CD72 (74), an inducible receptor on T cells (64), or CD5 itself through homophilic interactions between cells (75). CD5 may also bind and respond to IL-6 on B cells (76), as well as to fungal cell wall components (77). In the CD5ΔDC mice, the T cells that were induced in response to tumor challenge expressed lower levels of CD5 than WT DCs. This suggests that high expression of CD5 on T cells might be maintained through a homotypic interaction with CD5 on DCs (75). Alternatively, CD5 on DCs might interact with an unknown ligand on T cells that indirectly regulates CD5 expression on T cells. CD5 expression on the T cells in our tumor-bearing CD5ΔDC mice was reduced on the antigen-specific $CD8^+$ T cells, as well as on $CD4^+$ T cells in both LNs and tumors. The impact of this low CD5 expression might translate directly into a reduction in the helper or effector functions that are required for successful tumor rejection in response to ICB therapy (46) or into poor licensing of cDC1s (45), which ultimately has a negative impact on CTL-mediated antitumor immunity.

Taken together, our findings highlight the requirement of the $CD5^+$ DC population for directing antitumor $CD4^+$ and $CD8^+$ T cell immunity. Furthermore, $CD1c^+CD5^+$ DC abundance in human lymphoid tissue might serve as a biomarker not only of T cell effector quality but also of responsiveness to ICB therapy. Classifying the TME based on the immune infiltrate has predictive power (78). Thus, in addition to recent efforts to identify distinctive patient TMEs (38, 79, 80), our unbiased, high-dimensional analytic approach has identified CD5 expression on DCs as a valuable component that could facilitate the design of treatment protocols and may help identify patients that are poised for a therapeutic response.

Materials and methods summary

Tissue specimens

Human tissues (including skin, blood, and peripheral lymphoid organs) were obtained from healthy volunteers and patients with melanoma who underwent cosmetic and therapeutic surgical procedures at Washington University in St. Louis and Barnes-Jewish Hospital in accordance with the guidelines of the institutional review board (IRB). Samples were processed immediately, and cell subsets were isolated. A written informed consent was obtained in accordance with the guidelines of the IRB from patients with melanoma as well as healthy donors who donated skin and whole blood (listed in table S1).

Human DC subsets

Human tissue DCs were isolated from tissues using mechanical and enzymatic methods followed by fluorescence-activated cell sorting (FACS) as needed. Human DCs were also generated in vitro from monocytes or from cord blood–derived $CD34^+$ HPCs with GM-CSF, Fms-like tyrosine kinase receptor 3 ligand (FLT3-L), and stem cell factor (SCF). Where noted, IL-6 and IL-23 were added at the indicated concentrations, as described previously (18) and in (44).

Correlating CD5 expression with disease prognosis

TCGA level 3 normalized RNA-seq–based expression for 26 cancer types was assessed using the University of California, Santa Cruz (UCSC) Xena Browser. Survival analysis was performed using mRNA data to obtain high and low binary variables for *CD5* and $CD5^+$ DC signature expression. Hazard ratios were calculated using the Cox proportional hazard model.

scRNA-seq of live $CD45^+HLA\text{-}DR^+$ cells, sorted from iLNs and uLNs by using the Chromium Single Cell 3′ Reagent Kit v3, was used to identify different myeloid cell types and specific gene signatures for each cluster. For such identification, the R package Seurat (version 3.1.2) was used to analyze the digital expression matrix generated from raw reads aligned to the human genome (hg38). Principal components analysis (PCA), t-distributed stochastic

neighbor embedding (t-SNE), and UMAP were used to reduce the dimensions of the data, and the first two dimensions were used in plots. The "FindClusters" function was later used to cluster the cells. To measure the relative abundance of *CD5* expression, the total expression was calculated for each myeloid cluster separated by tumor-involved and tumor-uninolved samples.

Human DC and T cell cocultures

To elucidate the effects of CD5-expression on DCs or T cells to the magnitude of the T cell response, we sorted DCs based on their CD5 expression; alternatively, CD5 expression was genetically altered using CRISPR and CRISPR-Cas9 technology. $CD5^+$ and $CD5^-$ DCs were then cocultured with autologous or allogeneic $CD4^+$ and $CD8^+$ T cells. Alternatively, we used hCD5ΔT cells or control T cells and cocultured with $CD5^+$ and $CD5^-$ DCs. Multiparameter flow cytometry was used for immunophenotyping and T cell proliferation assessment, and RNA-seq was used for gene expression evaluation for both DCs and T cells.

Murine CD5-deficient models

Using CRISPR-Cas9 technology, we generated mice with loxP insertions that flanked axons 2 and 9 of the *Cd5* locus. We then bred these $Cd5^{f/f}$ mice with mice that expressed Cre recombinase under the *Zbtb46*, *Itgax*, and *Cd4* promoters to delete CD5 in cDCs [CD5ΔDC (fig. S6)] and T cells [CD5ΔT (fig. S9)].

Tumor models and ICB therapy

MCA1956 (*81*) and MC-38 (*82*) lines were injected subcutaneously into the anatomical right flanks of mice (1×10^6 cells per mouse). Mice were treated intraperitoneally with anti–PD-1 or anti–CTLA-4 antibody (200 μg per mouse) every 3 days, starting at day 3 after tumor inoculation. The OVA-expressing MCA1956-mOVA line is spontaneously rejected by WT mice (*45*). Tumor growth was quantified by Vernier caliper measurements and expressed as the average of two perpendicular diameters. For tumor models, animals were injected at 8 to 10 weeks of age. All studies performed on mice were done in accordance with the Institutional Animal Care and Use Committee (IACUC) at Washington University in St. Louis. In accordance with our IACUC-approved protocol, maximal tumor diameter was 20 mm in one direction and in no experiments was this limit exceeded.

Full materials and methods are accessible in the supplementary materials (*44*).

REFERENCES AND NOTES

1. J. Larkin *et al*., Five-year survival with combined nivolumab and ipilimumab in advanced melanoma. *N. Engl. J. Med.* **381**, 1535–1546 (2019). doi: 10.1056/NEJMoa1910836; pmid: 31562797
2. I. Mellman, G. Coukos, G. Dranoff, Cancer immunotherapy comes of age. *Nature* **480**, 480–489 (2011). doi: 10.1038/nature10673; pmid: 22193102
3. R. M. Steinman, J. Banchereau, Taking dendritic cells into medicine. *Nature* **449**, 419–426 (2007). doi: 10.1038/nature06175; pmid: 17898760
4. J. Lee *et al*., Restricted dendritic cell and monocyte progenitors in human cord blood and bone marrow. *J. Exp. Med.* **212**, 385–399 (2015). doi: 10.1084/jem.20141442; pmid: 25687283
5. E. Klechevsky, Functional diversity of human dendritic cells. *Adv. Exp. Med. Biol.* **850**, 43–54 (2015). doi: 10.1007/978-3-319-15774-0_4; pmid: 26324345
6. E. Klechevsky *et al*., Functional specializations of human epidermal Langerhans cells and $CD14^+$ dermal dendritic cells. *Immunity* **29**, 497–510 (2008). doi: 10.1016/j.immuni.2008.07.013; pmid: 18789730
7. J. Banchereau *et al*., The differential production of cytokines by human Langerhans cells and dermal $CD14^+$ DCs controls CTL priming. *Blood* **119**, 5742–5749 (2012). doi: 10.1182/blood-2011-08-371245; pmid: 22535664
8. J. Banchereau *et al*., Immunoglobulin-like transcript receptors on human dermal $CD14^+$ dendritic cells act as a CD8-antagonist to control cytotoxic T cell priming. *Proc. Natl. Acad. Sci. U.S.A.* **109**, 18885–18890 (2012). doi: 10.1073/pnas.1205785109; pmid: 23112154
9. H. Fujita *et al*., Human Langerhans cells induce distinct IL-22-producing $CD4^+$ T cells lacking IL-17 production. *Proc. Natl. Acad. Sci. U.S.A.* **106**, 21795–21800 (2009). doi: 10.1073/pnas.0911472106; pmid: 19996179
10. S. J. Balin *et al*., Human antimicrobial cytotoxic T lymphocytes, defined by NK receptors and antimicrobial proteins, kill intracellular bacteria. *Sci. Immunol.* **3**, eaat7668 (2018). doi: 10.1126/sciimmunol.aat7668; pmid: 30171080
11. C. Caux *et al*., $CD34^+$ hematopoietic progenitors from human cord blood differentiate along two independent dendritic cell pathways in response to granulocyte-macrophage colony-stimulating factor plus tumor necrosis factor alpha: II. Functional analysis. *Blood* **90**, 1458–1470 (1997). doi: 10.1182/blood.V90.4.1458; pmid: 9269763
12. C. C. Chu *et al*., Resident CD141 $(BDCA3)^+$ dendritic cells in human skin produce IL-10 and induce regulatory T cells that suppress skin inflammation. *J. Exp. Med.* **209**, 935–945 (2012). doi: 10.1084/jem.20112583; pmid: 22547651
13. A. C. Villani *et al*., Single-cell RNA-seq reveals new types of human blood dendritic cells, monocytes, and progenitors. *Science* **356**, eaah4573 (2017). doi: 10.1126/science.aah4573; pmid: 28428369
14. D. Dudziak *et al*., Differential antigen processing by dendritic cell subsets in vivo. *Science* **315**, 107–111 (2007). doi: 10.1126/science.1136080; pmid: 17204652
15. A. D. Edwards *et al*., Relationships among murine $CD11c^{high}$ dendritic cell subsets as revealed by baseline gene expression patterns. *J. Immunol.* **171**, 47–60 (2003). doi: 10.4049/jimmunol.171.1.47; pmid: 12816982
16. Y. Kumamoto *et al*., $CD301b^+$ dermal dendritic cells drive T helper 2 cell-mediated immunity. *Immunity* **39**, 733–743 (2013). doi: 10.1016/j.immuni.2013.08.029; pmid: 24076051
17. K. L. Lewis *et al*., Notch2 receptor signaling controls functional differentiation of dendritic cells in the spleen and intestine. *Immunity* **35**, 780–791 (2011). doi: 10.1016/j.immuni.2011.08.013; pmid: 22018469
18. D. Korenfeld *et al*., A type of human skin dendritic cell marked by CD5 is associated with the development of inflammatory skin disease. *JCI Insight* **2**, e96101 (2017). doi: 10.1172/jci.insight.96101; pmid: 28931765
19. X. Yin *et al*., Human blood $CD1c^+$ dendritic cells encompass $CD5^{high}$ and $CD5^{low}$ subsets that differ significantly in phenotype, gene expression, and functions. *J. Immunol.* **198**, 1553–1564 (2017). doi: 10.4049/jimmunol.1600193; pmid: 28087664
20. J. L. Hope, B. Pulendran, S. P. Schoenberger, P. D. Katsikis, 1st International Conference on Human & Translational Immunology. *Nat. Immunol.* **18**, 1–4 (2017). doi: 10.1038/ni.3635; pmid: 27984565
21. U. Cytlak *et al*., Differential IRF8 transcription factor requirement defines two pathways of dendritic cell development in humans. *Immunity* **53**, 353–370.e8 (2020). doi: 10.1016/j.immuni.2020.07.003; pmid: 32735845
22. M. Crowley, K. Inaba, M. Witmer-Pack, R. M. Steinman, The cell surface of mouse dendritic cells: FACS analyses of dendritic cells from different tissues including thymus. *Cell. Immunol.* **118**, 108–125 (1989). doi: 10.1016/0008-8749(89)90361-4; pmid: 2910499
23. M. O'Keeffe *et al*., Mouse plasmacytoid cells: Long-lived cells, heterogeneous in surface phenotype and function, that differentiate into $CD8^+$ dendritic cells only after microbial stimulus. *J. Exp. Med.* **196**, 1307–1319 (2002). doi: 10.1084/jem.20021031; pmid: 12438422
24. C. Ardavin, K. Shortman, Cell surface marker analysis of mouse thymic dendritic cells. *Eur. J. Immunol.* **22**, 859–862 (1992). doi: 10.1002/eji.1830220334; pmid: 1347747
25. A. Tarakhovsky *et al*., A role for CD5 in TCR-mediated signal transduction and thymocyte selection. *Science* **269**, 535–537 (1995). doi: 10.1126/science.7542801; pmid: 7542801
26. G. Bikah, J. Carey, J. R. Ciallella, A. Tarakhovsky, S. Bondada, CD5-mediated negative regulation of antigen receptor-induced growth signals in B-1 B cells. *Science* **274**, 1906–1909 (1996). doi: 10.1126/science.274.5294.1906; pmid: 8943203
27. H. S. Azzam *et al*., CD5 expression is developmentally regulated by T cell receptor (TCR) signals and TCR avidity. *J. Exp. Med.* **188**, 2301–2311 (1998). doi: 10.1084/jem.188.12.2301; pmid: 9858516
28. D. Hawiger, R. F. Masilamani, E. Bettelli, V. K. Kuchroo, M. C. Nussenzweig, Immunological unresponsiveness characterized by increased expression of CD5 on peripheral T cells induced by dendritic cells in vivo. *Immunity* **20**, 695–705 (2004). doi: 10.1016/j.immuni.2004.05.002; pmid: 15189735
29. H. Li *et al*., CD5 on dendritic cells regulates $CD4^+$ and $CD8^+$ T cell activation and induction of immune responses. *PLOS ONE* **14**, e0222301 (2019). doi: 10.1371/journal.pone.0222301; pmid: 31491023
30. J. L. Ceuppens, M. L. Baroja, Monoclonal antibodies to the CD5 antigen can provide the necessary second signal for activation of isolated resting T cells by solid-phase-bound OKT3. *J. Immunol.* **137**, 1816–1821 (1986). doi: 10.4049/jimmunol.137.6.1816; pmid: 3091691
31. F. Spertini, W. Stohl, N. Ramesh, C. Moody, R. S. Geha, Induction of human T cell proliferation by a monoclonal antibody to CD5. *J. Immunol.* **146**, 47–52 (1991). doi: 10.4049/jimmunol.146.1.47; pmid: 1701800
32. P. Vandenberghe, J. L. Ceuppens, Immobilized anti-CD5 together with prolonged activation of protein kinase C induce interleukin 2-dependent T cell growth: Evidence for signal transduction through CD5. *Eur. J. Immunol.* **21**, 251–259 (1991). doi: 10.1002/eji.1830210203; pmid: 1705509
33. T. Stanton, T. L. Stevens, J. A. Ledbetter, D. Wofsy, Anti-Ly-1 antibody induces interleukin 2 release from T cells. *J. Immunol.* **136**, 1734–1737 (1986). doi: 10.4049/jimmunol.136.5.1734; pmid: 3081630
34. C. Wang *et al*., CD5L/AIM regulates lipid biosynthesis and restrains Th17 cell pathogenicity. *Cell* **163**, 1413–1427 (2015). doi: 10.1016/j.cell.2015.10.068; pmid: 26607793
35. J. de Wit *et al*., CD5 costimulation induces stable Th17 development by promoting IL-23R expression and sustained STAT3 activation. *Blood* **118**, 6107–6114 (2011). doi: 10.1182/blood-2011-05-352682; pmid: 21926348
36. C. A. Matson *et al*., CD5 dynamically calibrates basal NF-κB signaling in T cells during thymic development and peripheral activation. *Proc. Natl. Acad. Sci. U.S.A.* **117**, 14342–14353 (2020). doi: 10.1073/pnas.1922525117; pmid: 32513716
37. G. Blaize *et al*., CD5 signalosome coordinates antagonist TCR signals to control the generation of Treg cells induced by foreign antigens. *Proc. Natl. Acad. Sci. U.S.A.* **117**, 12969–12979 (2020). doi: 10.1073/pnas.1917182117; pmid: 32434911
38. Q. Zhang *et al*., Landscape and dynamics of single immune cells in hepatocellular carcinoma. *Cell* **179**, 829–845.e20 (2019). doi: 10.1016/j.cell.2019.10.003; pmid: 31675496
39. B. Maier *et al*., A conserved dendritic-cell regulatory program limits antitumour immunity. *Nature* **580**, 257–262 (2020). doi: 10.1038/s41586-020-2134-y; pmid: 32269339
40. M. N. Artyomov *et al*., Modular expression analysis reveals functional conservation between human Langerhans cells and mouse cross-priming dendritic cells. *J. Exp. Med.* **212**, 743–757 (2015). doi: 10.1084/jem.20131675; pmid: 25918340
41. R. Cabrita *et al*., Tertiary lymphoid structures improve immunotherapy and survival in melanoma. *Nature* **577**, 561–565 (2020). doi: 10.1038/s41586-019-1914-8; pmid: 31942071
42. J. Banchereau, R. M. Steinman, Dendritic cells and the control of immunity. *Nature* **392**, 245–252 (1998). doi: 10.1038/32588; pmid: 9521319
43. T. I. Jensen *et al*., Targeted regulation of transcription in primary cells using CRISPRa and CRISPRi. *Genome Res.* **31**, 2120–2130 (2021). doi: 10.1101/gr.275607.121; pmid: 34407984
44. See supplementary materials.
45. S. T. Ferris *et al*., cDC1 prime and are licensed by $CD4^+$ T cells to induce anti-tumour immunity. *Nature* **584**, 624–629 (2020). doi: 10.1038/s41586-020-2611-3; pmid: 32788723
46. E. Alspach *et al*., MHC-II neoantigens shape tumour immunity and response to immunotherapy. *Nature* **574**, 696–701 (2019). doi: 10.1038/s41586-019-1671-8; pmid: 31645760

47. R. O. Bak, D. P. Dever, M. H. Porteus, CRISPR/Cas9 genome editing in human hematopoietic stem cells. *Nat. Protoc.* **13**, 358–376 (2018). doi: 10.1038/nprot.2017.143; pmid: 29370156
48. O. Padilla *et al*., Genomic organization of the human *CD5* gene. *Immunogenetics* **51**, 993–1001 (2000). doi: 10.1007/s002510000235; pmid: 11061284
49. O. Lecomte, J. B. Bock, B. W. Birren, D. Vollrath, J. R. Parnes, Molecular linkage of the mouse CD5 and CD6 genes. *Immunogenetics* **44**, 385–390 (1996). doi: 10.1007/BF02602784; pmid: 8781125
50. M. Ogishi *et al*., Inherited PD-1 deficiency underlies tuberculosis and autoimmunity in a child. *Nat. Med.* **27**, 1646–1654 (2021). doi: 10.1038/s41591-021-01388-5; pmid: 34183838
51. D. Korenfeld *et al*., STAT3 gain-of-function mutations underlie deficiency in human nonclassical CD16$^+$ monocytes and CD141$^+$ dendritic cells. *J. Immunol.* **207**, 2423–2432 (2021). doi: 10.4049/jimmunol.2000841; pmid: 34654687
52. P. Chomarat, J. Banchereau, J. Davoust, A. K. Palucka, IL-6 switches the differentiation of monocytes from dendritic cells to macrophages. *Nat. Immunol.* **1**, 510–514 (2000). doi: 10.1038/82763; pmid: 11101873
53. S. Wang, L. Pang, Z. Liu, X. Meng, SERPINE1 associated with remodeling of the tumor microenvironment in colon cancer progression: A novel therapeutic target. *BMC Cancer* **21**, 767 (2021). doi: 10.1186/s12885-021-08536-7; pmid: 34215248
54. P. Tan *et al*., MMP25-AS1/hsa-miR-10a-5p/SERPINE1 axis as a novel prognostic biomarker associated with immune cell infiltration in KIRC. *Mol. Ther. Oncolytics* **22**, 307–325 (2021). doi: 10.1016/j.omto.2021.07.008; pmid: 34553021
55. A. Moreno-Manuel *et al*., CD5 and CD6 as immunoregulatory biomarkers in non-small cell lung cancer. *Transl. Lung Cancer Res.* **9**, 1074–1083 (2020). doi: 10.21037/tlcr-19-445; pmid: 32953486
56. M. C. Cenit *et al*., Analysis of ancestral and functionally relevant CD5 variants in systemic lupus erythematosus patients. *PLOS ONE* **9**, e113090 (2014). doi: 10.1371/journal.pone.0113090; pmid: 25402503
57. S. Casadó-Llombart *et al*., Gene variation impact on prostate cancer progression: Lymphocyte modulator, activation, and cell adhesion gene variant contribution. *Prostate* **82**, 1331–1337 (2022). doi: 10.1002/pros.24407; pmid: 35767366
58. M. Potrony *et al*., Inherited functional variants of the lymphocyte receptor CD5 influence melanoma survival. *Int. J. Cancer* **139**, 1297–1302 (2016). doi: 10.1002/ijc.30184; pmid: 27169428
59. K. E. Pauken *et al*., Epigenetic stability of exhausted T cells limits durability of reinvigoration by PD-1 blockade. *Science* **354**, 1160–1165 (2016). doi: 10.1126/science.aaf2807; pmid: 27789795
60. C. Peña-Rossi *et al*., Negative regulation of CD4 lineage development and responses by CD5. *J. Immunol.* **163**, 6494–6501 (1999). doi: 10.4049/jimmunol.163.12.6494; pmid: 10586041
61. K. Inaba *et al*., Efficient presentation of phagocytosed cellular fragments on the major histocompatibility complex class II products of dendritic cells. *J. Exp. Med.* **188**, 2163–2173 (1998). doi: 10.1084/jem.188.11.2163; pmid: 9841929
62. L. M. Wakim, M. J. Bevan, Cross-dressed dendritic cells drive memory CD8$^+$ T-cell activation after viral infection. *Nature* **471**, 629–632 (2011). doi: 10.1038/nature09863; pmid: 21455179
63. L. A. Smyth *et al*., Acquisition of MHC:peptide complexes by dendritic cells contributes to the generation of antiviral CD8$^+$ T cell immunity in vivo. *J. Immunol.* **189**, 2274–2282 (2012). doi: 10.4049/jimmunol.1200664; pmid: 22821960
64. L. Biancone *et al*., Identification of a novel inducible cell-surface ligand of CD5 on activated lymphocytes. *J. Exp. Med.* **184**, 811–819 (1996). doi: 10.1084/jem.184.3.811; pmid: 9064341
65. J. N. Mandl, J. P. Monteiro, N. Vrisekoop, R. N. Germain, T cell-positive selection uses self-ligand binding strength to optimize repertoire recognition of foreign antigens. *Immunity* **38**, 263–274 (2013). doi: 10.1016/j.immuni.2012.09.011; pmid: 23290521
66. S. P. Persaud, C. R. Parker, W. L. Lo, K. S. Weber, P. M. Allen, Intrinsic CD4$^+$ T cell sensitivity and response to a pathogen are set and sustained by avidity for thymic and peripheral complexes of self peptide and MHC. *Nat. Immunol.* **15**, 266–274 (2014). doi: 10.1038/ni.2822; pmid: 24487322
67. R. B. Fulton *et al*., The TCR's sensitivity to self peptide-MHC dictates the ability of naive CD8$^+$ T cells to respond to foreign antigens. *Nat. Immunol.* **16**, 107–117 (2015). doi: 10.1038/ni.3043; pmid: 25419629
68. K. S. Weber *et al*., Distinct CD4$^+$ helper T cells involved in primary and secondary responses to infection. *Proc. Natl. Acad. Sci. U.S.A.* **109**, 9511–9516 (2012). doi: 10.1073/pnas.1202408109; pmid: 22645349
69. W. C. Kieper, J. T. Burghardt, C. D. Surh, A role for TCR affinity in regulating naive T cell homeostasis. *J. Immunol.* **172**, 40–44 (2004). doi: 10.4049/jimmunol.172.1.40; pmid: 14688307
70. D. Rogers *et al*., Pre-existing chromatin accessibility and gene expression differences among naive CD4$^+$ T cells influence effector potential. *Cell Rep.* **37**, 110064 (2021). doi: 10.1016/j.celrep.2021.110064; pmid: 34852223
71. C. E. Nelson *et al*., Reprogramming responsiveness to checkpoint blockade in dysfunctional CD8 T cells. *Proc. Natl. Acad. Sci. U.S.A.* **116**, 2640–2645 (2019). doi: 10.1073/pnas.1810326116; pmid: 30679280
72. G. Dorothée *et al*., In situ sensory adaptation of tumor-infiltrating T lymphocytes to peptide-MHC levels elicits strong antitumor reactivity. *J. Immunol.* **174**, 6888–6897 (2005). doi: 10.4049/jimmunol.174.11.6888; pmid: 15905531
73. M. M. Meredith *et al*., Expression of the zinc finger transcription factor zDC (Zbtb46, Btbd4) defines the classical dendritic cell lineage. *J. Exp. Med.* **209**, 1153–1165 (2012). doi: 10.1084/jem.20112675; pmid: 22615130
74. H. Van de Velde, I. von Hoegen, W. Luo, J. R. Parnes, K. Thielemans, The B-cell surface protein CD72/Lyb-2 is the ligand for CD5. *Nature* **351**, 662–665 (1991). doi: 10.1038/351662a0; pmid: 1711157
75. M. H. Brown, E. Lacey, A ligand for CD5 is CD5. *J. Immunol.* **185**, 6068–6074 (2010). doi: 10.4049/jimmunol.0903823; pmid: 20952682
76. C. Zhang *et al*., CD5 binds to interleukin-6 and induces a feed-forward loop with the transcription factor STAT3 in B cells to promote cancer. *Immunity* **44**, 913–923 (2016). doi: 10.1016/j.immuni.2016.04.003; pmid: 27096320
77. J. Vera *et al*., The CD5 ectodomain interacts with conserved fungal cell wall components and protects from zymosan-induced septic shock-like syndrome. *Proc. Natl. Acad. Sci. U.S.A.* **106**, 1506–1511 (2009). doi: 10.1073/pnas.0805846106; pmid: 19141631
78. M. Binnewies *et al*., Understanding the tumor immune microenvironment (TIME) for effective therapy. *Nat. Med.* **24**, 541–550 (2018). doi: 10.1038/s41591-018-0014-x; pmid: 29686425
79. Y. P. Chen *et al*., Single-cell transcriptomics reveals regulators underlying immune cell diversity and immune subtypes associated with prognosis in nasopharyngeal carcinoma. *Cell Res.* **30**, 1024–1042 (2020). doi: 10.1038/s41422-020-0374-x; pmid: 32686767
80. A. J. Combes *et al*., Discovering dominant tumor immune archetypes in a pan-cancer census. *Cell* **185**, 184–203.e19 (2022). doi: 10.1016/j.cell.2021.12.004; pmid: 34963056
81. H. Matsushita *et al*., Cancer exome analysis reveals a T-cell-dependent mechanism of cancer immunoediting. *Nature* **482**, 400–404 (2012). doi: 10.1038/nature10755; pmid: 22318521
82. T. H. Corbett, D. P. Griswold Jr., B. J. Roberts, J. C. Peckham, F. M. Schabel Jr., Tumor induction relationships in development of transplantable cancers of the colon in mice for chemotherapy assays, with a note on carcinogen structure. *Cancer Res.* **35**, 2434–2439 (1975). pmid: 1149045

ACKNOWLEDGMENTS

We thank the McDonnell Genome Institute at Washington University for sequencing; E. M. Lantelme, D. Brinja, and the Flow Cytometry Core at Washington University for cell sorting; X. Cui, M. Sentmamat, and the Genome Engineering and iPSC Center (GEiC) for human and mouse sgRNA design and validation; A. Burroughs for technical help; Y. Tao for biostatistical analysis; M. Diamond, J. Kipnis, G. Amarashinghe, and S. Stewart for helpful discussions; K. Ravichandran for critical reading of the manuscript; M. Bambouskova and N. Wiggie for help with experiments; D. Kreamalmeyer and R. Meade for mouse breeding and care; M. Colonna, S. Gilfillan, and M. Molgora for OT-I mice and the MC-38 cell line; M. Cella for providing access to tissue specimens and guidance; C.-S. Hsieh and J. Yi for OT-II mice; K. Murphy for providing access to the MCA1956-mOVA line; T. Saito from RIKEN (the Institute of Physical and Chemical Research, Japan) for providing the NFAT-expressing 2B4 cell line (43-1); T. Keller, H. Marsh, and M. Yellin from Celldex Therapeutics for providing CDX-301; and the surgeons, residents, nurses, and staff at Barnes-Jewish Hospital and the Washington University School of Medicine in St. Louis Department of Surgery for providing access to skin and melanoma specimens. Aspects of the studies, including tetramer production and flow cytometry analysis, were performed with the assistance of the Immunomonitoring Laboratory (IML), which is supported by the Andrew M. and Jane M. Bursky Center for Human Immunology and Immunotherapy Programs and the Alvin J. Siteman Comprehensive Cancer Center. We thank the Alvin J. Siteman Cancer Center at Washington University School of Medicine and Barnes-Jewish Hospital in St. Louis, MO, for the use of the GEiC and the IML. **Funding:** This work was funded by National Institutes of Health (NIH) grants 1R01CA245277-01A1 (E.K.), 5R01AR075959-02 (E.K.), and 5R21EB024767-03 (E.K.); and a National Psoriasis Foundation Translational Research Grant (E.K.). C.S. was supported in part by a postdoctoral training grant from NIH T32 CA009547-34 (R.D.S.). The Siteman Cancer Center is supported in part by National Cancer Institute (NCI) Cancer Center Support Grant #P30 CA091842. T.I.J. was funded by a grant from Novo Nordisk (NNF17OC0028894). Partial salary support for R.L.M. was provided by NIH grants R01 AI022553, R01 AR040312, R01 AR073252, R01 AR074302, R01 AI166313, and P50 AR080594. **Author contributions:** M.H., K.R., C.S., V.G., Y.Z., H.B., and L.G. performed experiments and analyzed the data; C.A.I., K.S., D.K., A.U.A., S.D., and D.D. provided technical help and performed experiments; F.M. and N.B. performed in silico analysis; M.W., J.G., T.I.J., R.B., C.L.A., and A.S. generated reagents; S.F. provided the MCA1956-mOVA cell line; J.L. performed biostatistical analysis; P.M.A. provided mice; R.D.S. provided the MCA1956 cell line; R.C.F. and T.T. provided patient specimens; M.W., M.M.G., M.P., R.L.M., R.B., R.D.S., and P.M.A. provided expertise; and E.K. conceived and performed experiments, analyzed and interpreted data, and wrote the manuscript. **Competing interests:** R.D.S. is a cofounder, scientific advisory board member, stockholder, and royalty recipient of Jounce Therapeutics and Neon Therapeutics and is a scientific advisory board member for A2 Biotherapeutics, BioLegend, Codiak Biosciences, Constellation Pharmaceuticals, NGM Biopharmaceuticals, and Sensei Biotherapeutics. R.B. is a cofounder, stockholder, and part-time employee of UNIKUM Therapeutics. All other authors declare that they have no competing interests. **Data and materials availability:** Single-cell data are available at Gene Expression Omnibus (GEO) under accession number (GSE219197). All other data are available in the manuscript or the supplementary materials.

SUPPLEMENTARY MATERIALS

View/request a protocol for this paper from *Bio-protocol*.

Submitted 2 February 2021; resubmitted 14 September 2022
Accepted 17 January 2023
10.1126/science.abg2752